Materials Horizons

ROYAL SOCIETY OF CHEMISTRY

REVIEW

View Article Online
View Journal | View Issue

Check for updates

Cite this: *Mater. Horiz.*, 2023, **10**, 1969

All-inorganic lead halide perovskite nanocrystals applied in advanced display devices

Liuli Yang,†[a] Jianhua Huang,†[a] Yike Tan,[a] Wei Lu,[a] Ziwei Li*[ab] and Anlian Pan *[a]

Advanced display devices are in greater demand due to their large color gamut, high color purity, ultrahigh visual resolution, and small size pixels. All-inorganic lead halide perovskite (AILHP) nanocrystals (NCs) possess inherent advantages such as narrow emission width, saturated color, and flexible integration, and have been developed as functional films, light sources, backlight components, and display panels. However, some drawbacks still restrict the practical application of advanced display devices based on AILHP NCs, including working stability, large-scale synthesis, and cost. In this review, we focus on AILHP NCs, review the recent progress in materials synthesis, stability improvement, patterning techniques, and device application. We also highlight the important role of materials systems in creating advanced display devices, followed by the challenges and opportunities in industrial processes. This review provides beneficial inspiration for the future development of AILHP NCs in colorful and white backlight, as well as high resolution full-color displays.

Received 15th January 2023,
Accepted 13th March 2023

DOI: 10.1039/d3mh00062a

rsc.li/materials-horizons

Published on 29 March 2023. Downloaded by Yunnan University on 8/16/2025 4:33:01 AM.

1. Introduction

The world has stepped into the modern information age with the rapid development of the electronic information industry, where display technology has become the most important information carrier in our daily lives for studying, working and entertainment activity. The development of display technology in the recent 20 years has undergone tremendous changes, from Cathode Ray Tubes (CRTs), to Liquid Crystal Displays (LCDs), leaving Plasma Display Panels (PDPs), entering into Light Emitting Diodes (LEDs) and Organic Light Emitting Diodes (OLEDs).[1–5] Although OLED technology fires an industrial revolution bringing flexible or collapse screen productions into public views, the inherent properties of organic materials are still an obstacle to obtain ultrahigh lightness displays, which limits the application and reduces the user experience in many application scenarios, like exercising in sports or watching under intense sunlight irradiation.[6–8] With the high requirement of display quality in wide color gamut, high brightness, pure color, and long lifetimes, nanocrystal (NC) or quantum dot (QD) based light-emitting devices hold great potential in next-generation advanced display devices, which are gradually walking into thousands of households.[9–16]

The working mechanism of QD-based display technology can be divided into two types: color-conversion light-emitting displays (QLEDs) assisted by QD color conversion layers and self-emissive light-emitting displays (QD-LEDs) supported by electroluminescence (EL) QD luminous layers.[17–22] In the framework of a QLED device, blue LEDs are adopted combined with down-conversion luminescence materials of QDs as the backlight, and other components of polarization filters, thin-film transistors and liquid crystals are utilized for the precise control of light emission.[23,24] This strategy usually provides economical technical solutions for low-value products, and their weaknesses, such as light leak and limited gamut, are serious barriers for their wide-range applications.[25,26] For QD-LED devices, light emissions are usually generated from LED devices driven by the control of current, and QDs are chosen as EL luminous materials with suitably designed neighboring layers injecting electrons and holes.[27,28] Each light-emitting unit in a large-area region can be controlled independently in this kind of technology resulting in high-contrast displays, and high-quality luminous materials help to realize the high-purity color and the wide color gamut.[29–31] But the industry procedure and technology are not mature now, and they still face problems in realizing both stable materials and low-cost manufacturing.

At present, mainstream commercial luminous materials are mainly based on YAG:Ce^{3+}, which lacks the red component resulting in a relatively low color rendering index (CRI, less than 75).[32] Semiconductor NCs or QDs have unique optical and optoelectronic properties, which have been developed from the 1990s, and the first prototype device based on CdSe NCs was reported to realize electrically triggered light emission in 1994.[33–36] After years of great efforts, CdS, ZnS and InP based colloidal QDs become the mainstream luminous materials of QD-LEDs, which show over 20%

[a] *Key Laboratory for Micro-Nano Physics and Technology of Hunan Province, Hunan Institute of Optoelectronic Integration, State Key Laboratory of Chemo/Biosensing and Chemometrics, College of Materials Science and Engineering, Hunan University, Changsha 410082, P. R. China. E-mail: anlian.pan@hnu.edu.cn*

[b] *Wuhan National Laboratory for Optoelectronics and School of Physics, Huazhong University of Science and Technology, Wuhan, China*

† These two authors are contributed equally.

Published on 29 March 2023. Downloaded by Yunnan University on 8/16/2025 4:33:01 AM.

external quantum efficiency (EQE) and an extremely long lifetime of a million hours for red, green and blue (RGB) devices.[37–42] But, the color gamut (Rec. 2020) display device based on colloidal QDs is always below 90% due to their inhomogeneous size and imperfect material quality. Besides, to achieve a high optical output efficiency, the design and the preparation of multi-level core–shell structures require complex and time-consuming processes. In 2015, all-inorganic lead halide perovskite (AILHP) NCs synthesized by the hot-injection method were first reported.[14] Beyond colloidal NCs, AILHP QDs are usually synthesized *via* a simplified process, which present ultrahigh photo-quantum efficiency and excellent crystal quality for narrow-band luminescence.[43,44] Over the last 5 years, the EQE of AILHP LEDs (PeLED) has increased from 0.1 to over 20%, which makes the research of perovskite QDs and their devices such hotspot topics because of their inherent advantages, including high photoluminescence quantum efficiency (PLQY; up to nearly 100%), narrow full width at half maximum (FWHM, $<$20 nm) and tunable emissions over the entire visible spectrum (400–700 nm).[45–48] In the same period, different components of perovskite structures have been reported, where organic or organic–inorganic hybrid perovskites could be synthesized by inducing organic molecules into the lattice replacing the A-site of cations. The EQE of organic–inorganic hybrid PeLEDs has been reported to be up to 20% ($FAPbBr_3$-532 nm: 19.2%; $MAPbI_2Br$-620 nm: 20.3%).[49,50] However, due to the oversized A-site of cations, organic–inorganic hybrid perovskites usually present worse stability than AILHPs in moisture and air environments.

Recently, AILHP NCs have been considered more promising as important photoelectric conversion materials for display devices, especially in wearable or flexible display devices.[23,51,52] However, the development of future display devices still faces great challenges in materials synthesis, performance improvement, patterning techniques, and device design.[11,53–55] In this review, responding to critical demands in the display area, we review the recent progress in AILHP NCs, focusing on the synthesis, stability improvement, fabrication technology, and application. This review begins with the basic synthesis of AILHP NCs and the key issues hindering their stability improvements. Next, we summarize and clarify the fabrication techniques in realizing scalable complex patterns, which is a significant step towards industry application. Then, recent remarkable processes on advanced PeLEDs are introduced with the combination of AILHP NCs in LCDs, LEDs, and micro-LEDs. Finally, the perspective and the commentary on opportunities and challenges of NC materials and their display applications are presented, which guide the way of multi-functionalization and intellectualization development in the future. This work reviews the development of AILHP NCs and related display devices, which provides beneficial inspiration for their applications in future display solutions.

2. Main structures of NC-based display devices

NC (QD) materials and their technology have been selected as commercial options for new-type QD-LCDs and QD-LEDs, which are represented by the products released by Samsung, QD Vision, and Nanosys.[56] The exploration on the development of advanced display devices based on perovskite NCs (QDs) has attracted great attention among academic and industrial circles. Here, various approaches to generating colorful light-emitting devices based on AILHP NCs (QDs) have been classified, and we will introduce the structure and the mechanism in four main models. This is needed to clarify that NCs and QDs are both nanomaterials with diameters in the range of tens or hundreds of nanometers, and NCs with single grain domain and tiny size ($<$20 nm) are further defined as QDs in this review.

Model 1 is the combination of an AILHP NC film and a blue LED, as illustrated in Fig. 1a. As a layer of color conversion, the NC films with different components (Br or I ions) partially absorb the blue light from the LED chip and transmit green or red light on the emitting side.[57] The structurally and spectrally stable AILHP NC solutions with batch fabrication are further made into uniform optical films covering the backlight LED, like pure color conversion films (red or green) or white-light-films of the backlight. Model 1 provides a feasible and low-cost solution for high color conversion and purity, which has achieved great commercial success in making a traditional low-value LCD screen showing pure colors. However, it also has some disadvantages that commercial color conversion layers lack the component of a high-quality red illuminant causing a low CRI.[58]

Model 2, similar to Model 1, uses blue micro-LEDs to stimulate AILHP NC films to obtain colorful light, for which the NC solution should be spin-coated or micro/nano-patterned onto the blue micro-LED chips. The resolution and pattern precision should meet the demand of the device size of micro-LEDs (5–50 μm), thus, new fabrication techniques have been explored in addition to QD photoresist, laser-writing and surface modification of the chip. AILHP NCs are promising for highly efficient color conversion and flexible pattern fabrication, and are the only emitters that can fully satisfy the required colour gamut (Rec. 2020) for ultra-high definition displays at low cost. But, they still face challenges in high-resolution patterns with desirable thickness (5–50 μm), which should be concluded as interdisciplinary problems.

Model 3 is a typical PeLED structure, containing top- and down-electrodes, electron (ETL) and hole (HTL) transport layers, and luminous AILHP NCs (Fig. 1b).[59] Designing suitable ETLs and HTLs plays an important role in creating highly efficient PeLEDs, which can induce suitable energy levels adjusting the large barriers between electrodes and luminous layers. There are several interfaces that electrons and holes should pass through to meet together and recombine as an emission photon, achieving the EL. The flatness of the interface and the quality of grain boundaries in each layer should be well improved to achieve remarkable performances. PeLEDs can be lighted by direct current voltage as well as the high frequency alternating current.

Model 4 is the framework of a PeLED based on a mini-/micro-LED, which is the reduced size of Model 3. To meet the market demand of display devices exhibiting higher resolution

 This journal is © The Royal Society of Chemistry 2023

Published on 29 March 2023. Downloaded by Yunnan University on 8/16/2025 4:33:01 AM.

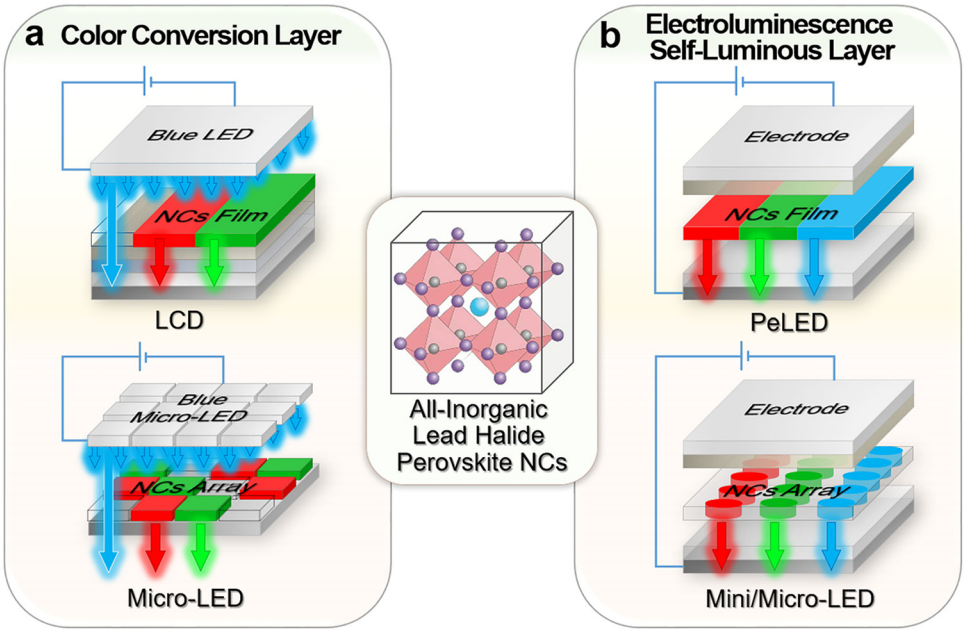

Fig. 1 General approaches for advanced display devices based on perovskite NCs. (a) Perovskite NCs as color conversion layers integrated in LCDs and micro-LEDs. (b) Perovskite NCs as EL luminous layers working in PeLEDs and mini/micro-LEDs.

(4 K or 8 K) in the same area of display screens, that means, when the LED size is reduced by half, the integration density or the display resolution is expected to be doubled. But, the control of each EL area should be separately achieved, which needs the help of complex integrated circuits, and it inevitably increases the process difficulty and the overall power consumption of the device.[60]

3. All-inorganic lead halide perovskite structures

AILHPs are commonly described by the chemical formula of ABX_3, where A^+ is a monovalent cation, B^{2+} is a divalent metal cation, and X^- is a single halide anion or the mixture of halides anions.[61,62] X^- anion is a tunable site to be filled with Cl^-, Br^- or I^- for desired colors.[63,64] The morphology of AILHPs can be synthesized in controllable methods realizing abundant nanostructures, such as zero-dimensional QDs, one-dimensional nanowires, and two-dimensional nanoplates.[65–68] Notably, AILHP NCs or QDs exhibit inherent superiorities in terms of excellent luminescence performance (high PLQY, tunable emission and narrow emission), perfect compatibility (solid and flexible substrates), and facile synthesis (hot-injection, microwave irradiation and supersaturated recrystallization).[28,69–75] These characteristics originate from unique structural attributes, which make AILHP NCs a promising candidate in advanced displays; here, mainstream synthesis methods for the morphology control and the performance improvement are discussed.

3.1 Nanocrystals and quantum dots

In the structural framework of ABX_3, X^- anions are present in large amounts among three chemical elements, and decide the photonic band gap of the luminous material.[76] The reaction of ion-exchange commonly occurs in material preparation.[77–79] Cation-exchange is facile and common, while anion-exchange reactions are uncommon in AILHP QDs. As is known, the remarkably fast anion-exchange could be accomplished in $CsPbX_3$ NC solution. By the rational design of reaction temperature, partial or complete anion-exchange could be controlled, which helped to synthesize pure-phase $CsPbX_3$ and uniform $CsPb(Cl/Br)_3$ or $CsPb(Br/I)_3$ compositions.[13] Besides, the anion-exchange reaction of AILHPs could also take place entirely in the solid state, as shown in Fig. 2a. By modulating the ratio of halide embedding in the salt matrix (KCl, KBr, and KI), the bright fluorescence of $CsPbX_3$ (X = Cl, Br, or I) NCs can be tuned over a wide spectral range (400–700 nm), maintaining the initial PLQY of ~80% and the narrow FWHM of 30–55 nm.[80]

The mainstream synthesis strategy of AILHP QDs should be the hot-injection method, which is based on ionic metathesis. During a one-step process, a precursor (*e.g.* Cs-oleate) was quickly injected into Pb/X hot solution (140–200 °C) to synthesize the monodisperse AILHP QDs, where PbX_2, octadecene, and oleic acid (OA)/oleylamine (OLA) are typically used as the solute, solvent, and ligands, respectively.[81,82] With the rational selection of precursors and the optimization of other process parameters, including the ligand and the reaction temperature, AILHP QDs with various compositions, sizes and shapes can be synthesized and modulated flexibly (Fig. 2b).[83–87] The monodisperse AILHP QDs had been synthesized by reacting Cs-oleate with appropriate ratios of PbX_2 salts in a high boiling solvent, whose emission properties were characterized showing narrow emission line widths of 12–42 nm, high quantum yields of 50–90%, and short radiative lifetimes of 1–29 ns.[14]

After the hot-injection process, some NCs are not stable due to their considerable defects, which are usually serious in red

Published on 29 March 2023. Downloaded by Yunnan University on 8/16/2025 4:33:01 AM.

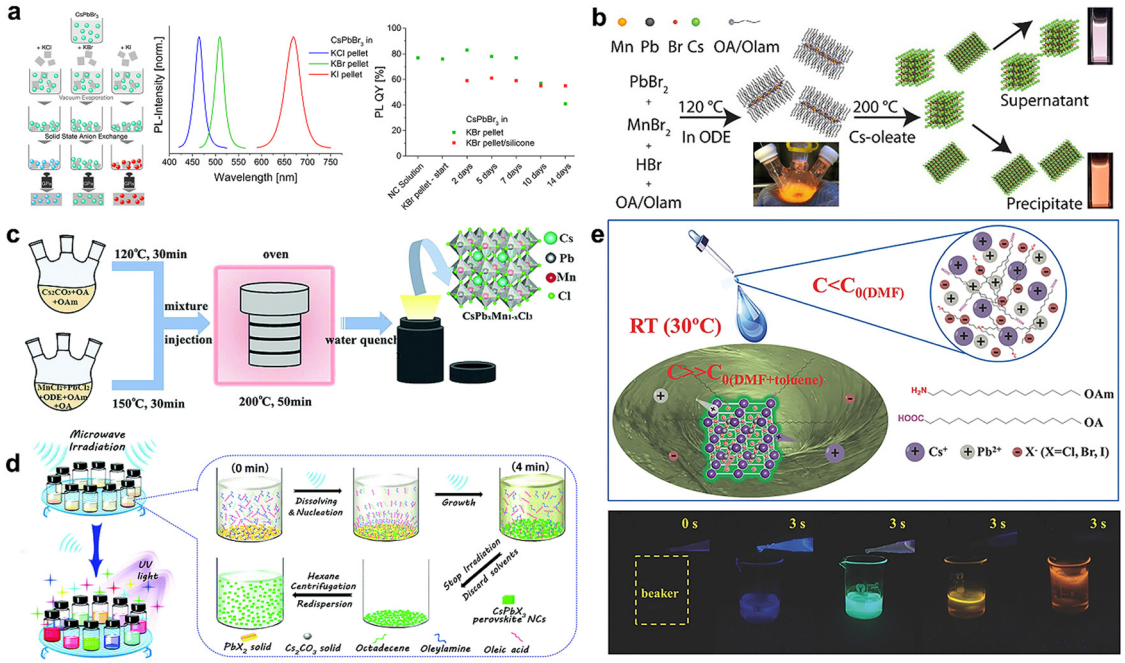

Fig. 2 Structure and synthesis method of $CsPbX_3$ QDs. (a) Controllable anion-exchange for preparing $CsPbX_3$ QDs with tunable colors. Reprinted with permission from ref. 80. Copyright 2016, American Chemical Society. (b) Direct hot-injection synthesis of Mn-doped $CsPbBr_3$ NCs. Reprinted with permission from ref. 87. Copyright 2018, American Chemical Society. (c) Preparation of Mn-doped $CsPbCl_3$ NCs by the solvothermal method. Reprinted with permission from ref. 88. Copyright 2018, Royal Society of Chemistry. (d) Controllable synthesis of $CsPbX_3$ NCs with tunable properties and morphologies by simple microwave irradiation. Reprinted with permission from ref. 74. Copyright 2017, Royal Society of Chemistry. (e) Fabrication of $CsPbX_3$ QDs with a high fluorescence quantum yield by supersaturated recrystallization. Reprinted with permission from ref. 75. Copyright 2016, Royal Society of Chemistry.

AILHP QDs. By mixing the Cs-oleate precursor solution and $PbCl_2/MnCl_2$ mixture into the reaction oven, doping elements could be induced by incorporating the hot-injection process, and it was demonstrated that Mn-doped $CsPbCl_3$ NCs had better stability than those synthesized using the traditional hot injection strategy (Fig. 2c).[88] Similarly, by introducing SnX_2 and BiX_3 into the reaction solvent, Sn- and Bi-doped AILHP QDs had been synthesized successfully. Element-doping helped to improve the structural and spectral stabilities, and also reduced the excessive usage of toxic elements.[89,90]

For the hot-injection synthesis of AILHP NCs, the experiment process should be conducted under high temperatures, water-free and oxygen-free conditions. Synthesized QDs are often observed with broadened size distributions, which should be attributed to the extremely fast and uneasily controllable crystallization caused by thermal gradients.[14] In recent reports, some novel and easy methods have been presented to prepare AILHP NCs, including microwave irradiation, ligand-assisted reprecipitation (LARP), supersaturation recrystallization, and the template strategy.

Fig. 2d shows the one-step microwave irradiation method to synthesize multiple colloidal $CsPbX_3$ NCs with tunable properties and morphologies in few minutes, which was performed in a heterogeneous solid–liquid reaction system without precursor preparation. With good stability and repeatability, this method was flexible for large-scale AILHP NC preparation and also suitable for constructing display devices.[74] In the approach of LARP, perovskite precursors dissolved in a good solvent (such as dimethylsulfoxide (DMSO), *N*,*N*-dimethyl formamide (DMF), *etc.*), and a poor solvent (such as hexane, toluene, *etc.*) are subsequently dropped in solutions in the presence of alkylamine ligands, which helps to induce the formation of perovskites through supersaturation. The LARP technique has been widely used to synthesize the organic–inorganic hybrid lead halide perovskite, which does not require heating and an inert atmosphere. In 2015, small $MAPbBr_3$ QDs were first synthesized by this method showing a high PLQY of up to 70%.[91] Subsequently, this method has also been extended to AILHPs, namely supersaturated recrystallization, as shown in Fig. 2e. The core–shell structures of $CsPbX_3$ QDs could be prepared in a rapid process within 3 seconds, and their luminous characteristics aid in achieving a high quantum yield (up to $\approx$90%) and long-time photo-stability.[75] The key point of the supersaturated recrystallization process was achieved by using transfer various inorganic ions from their good into poor solvents, other than traditional strategy of solvent evaporation.

3.2 Nanostructures with special morphology

In the material system of AILHP nanostructures, their photophysical properties are highly dependent on the shape and morphology.[92,93] Many efforts have been devoted to exploring new synthetic approaches for higher morphological complexity beyond current mainstream methods. Fig. 3a shows the micromorphology of dodecapod-branched $CsPbX_3$ NCs and their

 This journal is © The Royal Society of Chemistry 2023

Published on 29 March 2023. Downloaded by Yunnan University on 8/16/2025 4:33:01 AM.

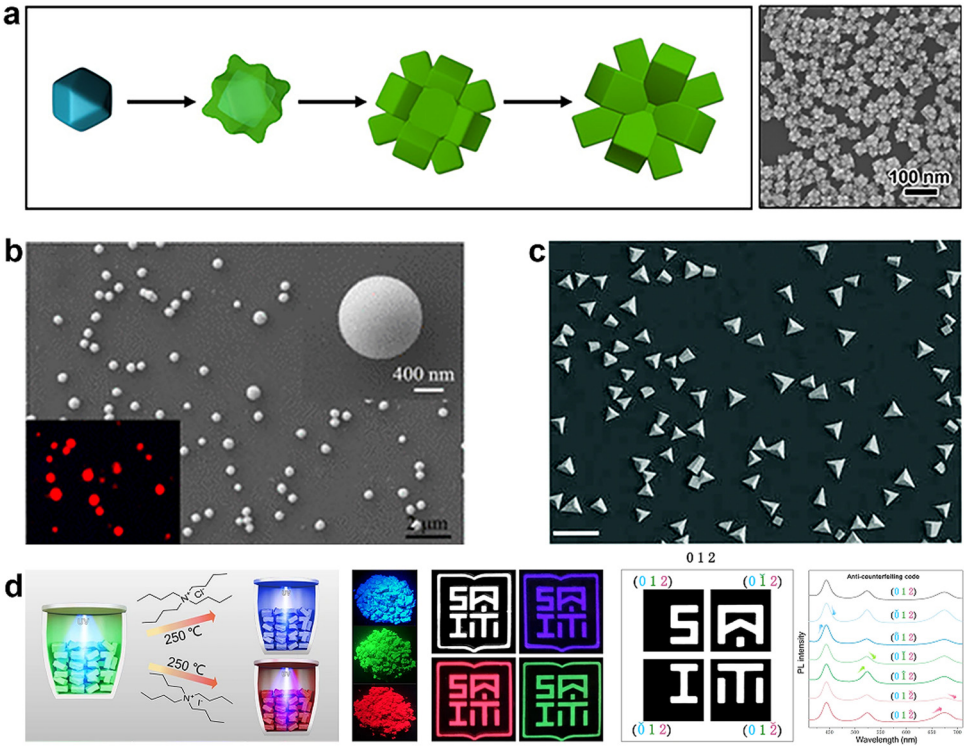

Fig. 3 Some AILHP nanostructures with special morphologies. (a) Controlled growth of dodecapod-branched $CsPbX_3$ NCs by the solvothermal process. Reprinted with permission from ref. 94. Copyright 2018, Royal Society of Chemistry. (b) SEM image of $CsPbX_3$ submicron spheres by CVD. Reprinted with permission from ref. 101. Copyright 2017, American Chemical Society. (c) SEM image of $CsPbBr_3$ tetrahedral synthesized by CVD. Reprinted with permission from ref. 102. Copyright 2019, Royal Society of Chemistry. (d) Schematic of the template-assisted synthesis of $CsPbX_3$ NCs. Reprinted with permission from ref. 105. Copyright 2022, Springer Nature.

growth diagram, where the critical step is the formation of cuboctahedral Cs_4PbBr_6 seeds in a Cs-rich environment, and followed by the phase transformation from Cs_4PbBr_6 to $CsPbBr_3$. The photoluminescence (PL) emission spectra of this kind of flower nanostructure could be varied covering the whole visible spectral range with a high PLQY (50%) and a narrow width (18 nm), which hold promise in the application of a white light-emitting device (WLED) exhibiting outstanding performance (135% of NTSC standard gamut).[94]

Chemical vapor deposition (CVD) growth is one of the popular techniques to synthesize low-dimensional materials, where reaction sources are placed at the end of the tube.[95–100] All-inorganic $CsPbX_3$ microspheres with tunable sizes (0.2–10 μm) were successfully fabricated by dual-source CVD, as shown in Fig. 3b, and the trick of forming the spherical shape is constructing surface tension forces at high temperature. An ultrahigh cavity quality factor (~6100) was recorded in these perfect photonic cavities, which, to the best of our knowledge, represents the highest performance of perovskite nanostructures.[101] Interestingly, in another work presented in Fig. 3c, single crystalline tetrahedron-shaped $CsPbBr_3$ structures were synthesized *via* the vapor growth method. The growth morphology could be related to the negatively charged surface of silica enabled surface cationic affinity, and other morphologies were also found due to the formation of varied shapes (nanorods and nanoplates) by connecting O atoms. The perfect structure and smooth surface help to obtain strong light–matter interactions for optical and photonic devices.[102]

The template-assisted preparation method has been widely reported in creating nanostructures with large areas and uniformity, and can also be employed for synthesizing AILHP NCs. By infiltrating perovskite precursor solutions into the pores of mesoporous silica matrixes, *meso*-SiO_2-templated $CsPbBr_3$ and hybrid perovskite NCs were prepared exhibiting an unprecedented high quality of PL, which is owing to the intrinsic tolerance of the electronic structure to the defects in these compounds.[103] Besides, due to the quantum confinement of the zeolite matrix, perovskite-zeolite composites have been reported to achieve efficient PL emission by passivating the defects of perovskite with H-bonding interaction.[104] These kinds of composites exhibit great potential to be largely applied in multicolor-coded anti-counterfeiting inks and backlight displays (Fig. 3d).[105–107]

4. Strategies for stability improvement

4.1 Ligand modification

AILHP NCs as a class of promising optoelectronic materials suffer from severe instability in chemical and phase transition, especially in air and humid environments. The traditional surface passivation strategy is building long-chain capping

Published on 29 March 2023. Downloaded by Yunnan University on 8/16/2025 4:33:01 AM.

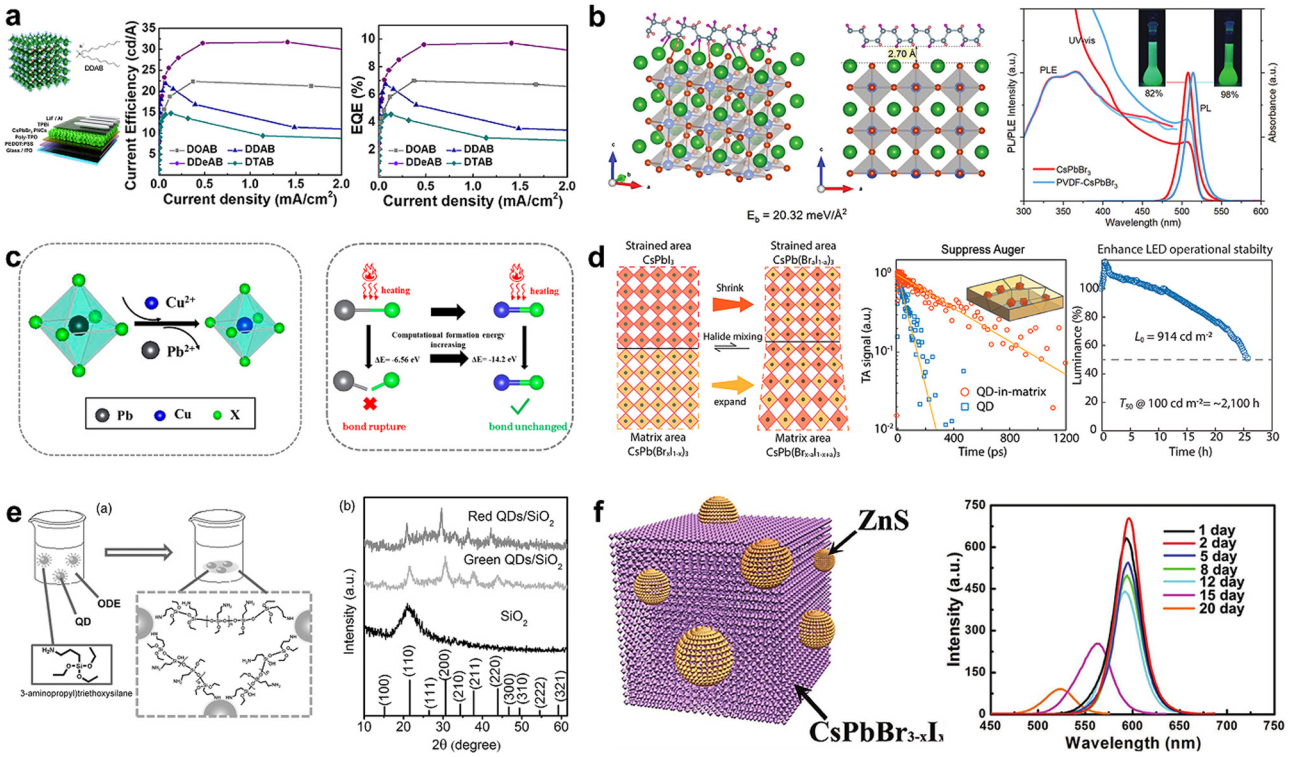

Fig. 4 Typical strategies for stability improvement of AILHP NCs. (a) Device performance of PeLEDs with the modification of DDAB-$CsPbBr_3$ NCs. Reprinted with permission from ref. 112. Copyright 2019, American Chemical Society. (b) The structure and spectra of PVDF-$CsPbBr_3$ QDs. Reprinted with permission from ref. 114. Copyright 2021, Royal Society of Chemistry. (c) Schematic diagram of the influence on thermal stability in Cu-doped $CsPbX_3$ QDs. Reprinted with permission from ref. 121. Copyright 2019, American Chemical Society. (d) Diagram, TA spectra and the operational lifetime of strain-tuned $CsPbI_3$ QDs-in-matrix. Reprinted with permission from ref. 133. Copyright 2021, American Chemical Society. (e) The formation of QD/silica composites and their XRD spectra. Reprinted with permission from ref. 146. Copyright 2021, Wiley-VCH. (f) Structure and optical stability of $CsPbBr_{3-x}I_x$/ZnS. Reprinted with permission from ref. 153. Copyright 2017, Wiley-VCH.

ligands, such as OA and OLA, and they can improve the structure and spectral stability of AILHP NCs. However, their insulating characteristics of long-chain ligands hinder the performance breakthrough in optoelectronic application. Recently, short-chain ligands have attracted more attention as surface passivators of AILHP NCs, which can bind tightly and densely with perovskites providing short carrier transport channels as better choices for display device applications.

Tightly binding the surface-capping ligands, such as soy lecithin and 3-(*N*,*N*-dimethyloctadecylammonio)-propanesulfonate, are suitable for long-term retention of the colloidal and structural integrity, which were designed for $CsPbX_3$ NCs to obtain high spectral performance and a large PLQY.[108,109] In 2018, tetraoctylammonium bromide (TOAB), didodecyldimethylammonium bromide (DDAB), and octanoic acid were reported to passivate QDs.[110] Benefitting from the synergy effect, the highest EQE of the prepared LED devices reached 11.6% due to the improved charge injection and transportation in QD films. In 2019, it was reported that SCN– as the ligand of $CsPbX_3$ NCs can reduce Pb^{2+} surface defects and improve the PLQY of material up to 25%.[111] In the same year, anther literature found that small ligands (DDAB) surrounding the surface of QDs could effectively passivate the nanocrystal surface and reduce the aggregation of QDs (Fig. 4a). A remarkable green LED recorded a current efficiency of 31.7 cd A^{-1} and an EQE of 9.7%, which is 16 times higher than that of PeLEDs with OLA ligands.[112] In 2020, DDAB was introduced to combine with the surface of QDs, and the effective passivation of surface defect helps to realize highly stable DDAB-$CsPbI_3$ NCs retaining a high PLQY (>80%) for more than two months.[113] In 2021, α-phase poly (vinylidene fluoride) (PVDF) was demonstrated as the surface-capping ligands prepared by a one-step microwave method, and the PLQY of PVDF-QDs reached up to 98%, which was much higher than that of pristine QDs with OA/OLA ligands (Fig. 4b).[114]

4.2 Ion doping

The synthesis reaction of NCs mostly occurs in solutions, and the reaction temperature, the inappropriate proportion of reaction sources, and the inherent energy system of materials decide that there still exist ineluctable defects in synthesized AILHP NCs. An ion doping strategy has become an important way to fill in defects and improve the structure stability. The structure of ABX_3 has three elements located at three different lattice positions, and they have various influences on the properties of the material. For example, $CsPbBr_3$ is a typical AILHP, where Cs has little effect on its electronic structure. However, the 4p orbital of Br and the 6p orbital of Pb mainly

 This journal is © The Royal Society of Chemistry 2023

Published on 29 March 2023. Downloaded by Yunnan University on 8/16/2025 4:33:01 AM.

decide the valence band and conduction band of the crystal, respectively.[115] The doping elements occupied in defects or substitutions may change the energy of conduction and valence bands, or induce new energy levels of impurity or defect, which both influence the luminescence kinetics and light colors of the materials.[116,117] Notably, the structural and spectral properties of NCs are more sensitive to the doping element, substitution density, and grain size.

The A-site has a great influence on the structure and stability of NCs, and alkali metals, such as Na^+,[118] K^+,[119] are expected to be ideal doping ions at the A-site. Besides, Rb^+ ions were reported to be introduced to dope $CsPbCl_3$, which reduced the defects resulting in a narrow FWHM and high PLQY.[120] For the B-site element, it mainly contributes to the conduction band of NCs having a great effect on their optoelectronic properties. Elements of Cu^{2+},[121,122] Zn^{2+},[123] Fe^{2+},[124,125] and Mn^{2+}[122,126] are commonly used as doped ions, and a suitable doping composition can limit the ion diffusion and improve the thermal stability and the optical properties of NCs, as shown in Fig. 4c.[121] Meanwhile, these B-site doping elements can reduce the lead content to a certain extent, which plays an active role in solving the problems of heavy lead and environmental toxicity. Recently, less rare earth elements of Eu^{3+},[127] Bi^{3+},[126,128] and Tm^{3+}[122] were demonstrated to improve the PLQY obviously.

X-element is quite important for tunable energy band and PL emission. By changing the halide ratio, $CsPbX_3$ QDs with various components show different emissions in the whole visible range.[129] The mixed-halide perovskites of $CsPb(Cl/Br)_3$ and $CsPb(Br/I)_3$ could be readily produced by varying the molar ratio of PbX_2 precursors, but the $CsPb(Cl/I)_3$ alloy could not be obtained owing to the large lattice mismatch.[14] Under the reaction mechanism of anion exchange, the optical bandgap can be tuned from 1.8 to 3.0 eV by varying the ratio of different halides.[130] Though a narrow FWHM and a high EQE have been widely reported from blue and green AILHP NCs, red AILHP NCs still face big problems in stable narrow PL due to the severe migration of halide ions.[131,132] Mn doping was introduced to drive the homogeneous crystallization of a $CsPb(Br_xI_{1-x})_3$ matrix, which reduced gradient crystallization and suppressed halide segregation simultaneously. Specifically, the QDs-in-matrix shows suppressed Auger bi-excition recombination and bright PL at high excitation, and the PeLED enables an operating half-life of 2400 h at an initial luminance of 100 cd m^{-2} (Fig. 4d).[133] Besides, a bromine-doping strategy with an additional PbI_2-recondition process was demonstrated to successfully synthesize highly stable $CsPbBr_{1.2}I_{1.8}$ QDs, and their structures were analyzed using point-to-point diffraction patterns.[134] The structures with rational composition not only can realize the confinement of ions preventing their migration, but also avoid the collapse and damage of the structure in the air or humid environment.[135–137] Moreover, composition regulation and band gap engineering have been widely reported in one-dimensional nanowires and quasi two-dimensional NCs.[138–141]

Ion doping is one of the positive modulation strategies to improve the stability of perovskite NCs. But in element-doped perovskites, there is still a passive influence of structure stability by the exchange of doped ions, which may get worse in high temperatures or under light irradiation. External disturbance can provide additional energy and momentum overcoming the weak confinement of chemical bonds with neighboring atoms, which may stimulate the movement of ions suppressing the recombination of excitons. The above-mentioned ion-doping is a powerful method to generate localized confinement for the control of ion-exchange. In recent years, the core–shell structure of perovskites has been prepared to build barrier blocks avoiding the anion exchange in lighting devices. For example, an AlO_x shell with adjustable thickness was demonstrated to prevent further anion-exchange reactions and improve the stability of NCs.[142]

4.3 Insulator coating

Compared with the ion doping and ligand modification strategies mentioned above, the strategy of coating is more straightforward to improve the performance by isolating water and oxygen.[143] So far, silica (SiO_2) is a good choice for passivating NCs due to its good light transmittance and excellent structural stability against environmental and chemical factors.[144,145] Usually, NCs were first formed in a water-free synthesis system, and then exposed to air to capture the water vapor, after the reaction with tetraethyl orthosilicate (TEOS) or 3-aminopropyl triethoxysilane (APTES), the core–shell structure of NC/silica composites could be realized (Fig. 4e).[146,147] These composites exhibited extremely high stability in air, and the anion-exchange reactions were not observed between neighboring QDs.[148] However, most reported NCs were large particles, in which multiple NCs were encapsulated into one SiO_2 shell particle, where uniformity in the thickness of the SiO_2 shell couldn't be maintained.[147,149] Under the motivation of meeting requirements in some important applications, the exploration of a single particle rather than big aggregates seems more promising for the future, and much effort has been devoted to developing the surface modification of AILHP NCs with oxides at a single particle level.[150,151] The coating of single QDs with SiO_2 not only retains the optical properties of luminescent materials, but also protects the materials from the dissolution by polar solvents.[152]

At present, the coating materials of AILHP NCs have been extended to a group of mesoporous materials, such as TiO_2, AlO_x, ZnS, and so on. $CsPbX_3$/ZnS heterostructures were prepared using a simple liquid-phase strategy, and NCs were maintained to be stable in the air for 12 days, as shown in Fig. 4f.[153] Monodisperse $CsPbBr_3/TiO_2$ nanocomposites were demonstrated to show excellent water stability and PL intensity.[154] In addition, atomic layer deposition (ALD) is an alternative method to realize the precision thickness control of alumina layer on $CsPbBr_3$ QDs.[155,156] Besides, SiO_2/Al_2O_3 monolith binary coating has been already synthesized on $CsPbBr_3$ QDs, which decreased the pinhole defects of coating layers beyond the individual coatings of SiO_2 or Al_2O_3.[157] Interestingly, monodisperse $CsPbX_3/SiO_2$ NCs were successfully prepared by combining a water-triggered transformation

Published on 29 March 2023. Downloaded by Yunnan University on 8/16/2025 4:33:01 AM.

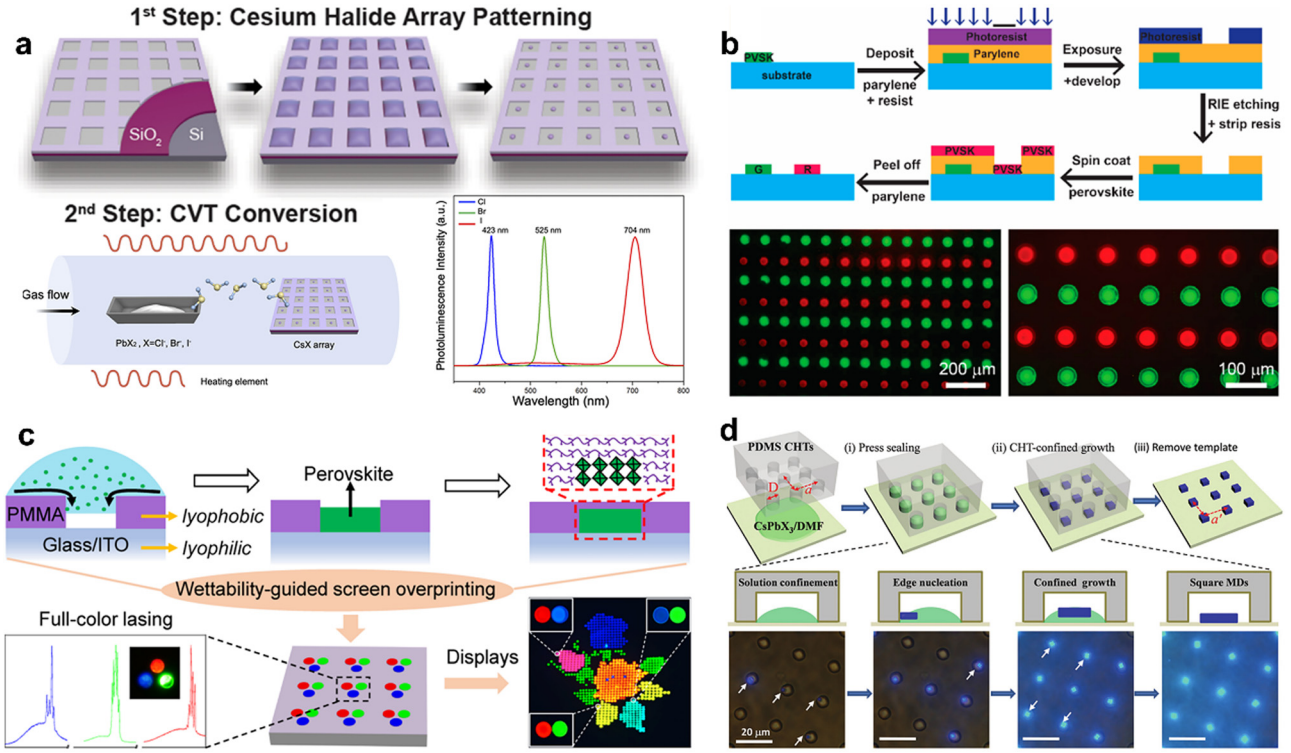

Fig. 5 Template-assisted patterning of AILHPs. (a) Schematics of large-scale preparation of perovskite arrays within a two-step patterning process. Reprinted with permission from ref. 159. Copyright 2020, American Chemical Society. (b) Schematic view of dry lift-off of large-scale perovskite patterns for multicolor display applications. Reprinted with permission from ref. 160. Copyright 2020, American Chemical Society. (c) Schematics of preparing full-color perovskite microdisk arrays by wettability-guided screen-overprinting. Reprinted with permission from ref. 163. Copyright 2022, American Chemical Society. (d) PDMS-confined solution-growth of $CsPbCl_3$ structures on a 0.2 mm thin quartz coverglass. Reprinted with permission from ref. 165. Copyright 2017, Wiley-VCH.

process and a sol–gel method. The quick separation of the product from the interface results in insufficient time for the nucleation and growth of silica, thus obtaining a half-coated $CsPbX_3/SiO_2$ Janus particles, which could be further controlled for surface modification.[158] Moreover, a novel three-dimensional (3D) direct lithography technique has been reported recently, that AILHP NCs in glass with tunable composition and bandgap could be reversibly fabricated by ultrafast laser-induced liquid phase separation, which provides a solid platform for optical storage, micro-LEDs, and holographic displays.[131]

5. Patterned perovskites

5.1 Template method

As a mature strategy, the template patterning method has been widely used in the field of optoelectronics to satisfy the requirement of artificial micro/nanostructures. The ability to create a periodic array structure is of central importance to extend the advanced display application of AILHPs towards commercialization. Template patterning means that an appropriate template substrate was first designed and prepared to guide the growth of AILHPs with special morphology and period. Fig. 5a shows the schematic view of a two-step patterning process, where CsX arrays were originally grown on a prepatterned surface, and then a chemical vapor transport (CVT) process was used to convert the CsX into $CsPbX_3$ perovskite arrays. Scalable single crystal inorganic halide perovskite arrays with a controllable crystal size (from 0.2 to 1.2 μm) and spacing (from 2 to 20 μm) were successfully reported emitting RGB PL at 423 nm, 525 nm and 704 nm, respectively.[159]

Photolithographic patterning is a fast and reproducible procedure to generate chip-scale micro/nanostructures. To solve the problem of developing the lift-off process avoiding etching perovskites, a dry lift-off process followed by standard photolithography was explored. Fig. 5b presents the schematic view of photolithography processes and the ability to create AILHP patterns with periodical structures and complex morphologies.[160] This strategy can even enable multicolor perovskite patterns by using the standard photolithography process for multiple times. To further decrease the linewidth of perovskite patterns, a top-down lithography fabrication procedure based on electron-beam lithography was developed.[161] Another work demonstrated the two-step fabrication of Cs_4PbBr_6 arrays within an all-solution process based on photolithography; furthermore, their potential application of photodetector arrays and flexible luminescence patterns were presented.[162]

An alternative strategy should be the wettability-guided screen-overprinting, which is a common technique in the industry of flexible electronics. In Fig. 5c, a novel universal

 This journal is © The Royal Society of Chemistry 2023

Published on 29 March 2023. Downloaded by Yunnan University on 8/16/2025 4:33:01 AM.

screen-overprinting process is shown, which is based on wet-solute-chemical dynamics involving a combination of surface tailoring and solvent selection. This is successful in integrating full-color perovskite microdisk arrays on a prepatterned template realizing the RGB display of a flower.[163] Another group demonstrated that perovskite microlasers could be precisely defined with controlled physical dimensions and spatial locations by such a wettability-guided screen-printing strategy, which was highly compatible with LED device architectures and was favorable for the mass production of micro-LED arrays.[164]

The nanoimprinting process is a well-known method to prepare micro/nanostructures guided by another patterned substrate with large-area uniform pressure, and it is commonly considered as a low-cost and high-efficient patterning method. Choosing suitable pre-patterned stamps with good thermal stability and pressure resistance is vital for the result of the nanoimprinting process. Polydimethylsiloxane (PDMS), polymethylmethacrylate (PMMA), SiO_2, and anodized aluminum oxide are popular candidates for pre-patterned stamps. A PDMS template with arrayed cylindrical holes was induced to confine the solution-growth for effective fabrication of single-crystal $CsPbX_3$ with large arrays (up to 1×1 cm^2), as shown in Fig. 5d.[165] In a similar work, the arrayed growth islands were realized by imprinting a precursor gel with PDMS stamps. Followed by the successive deposition of ZnO and Ag, well-aligned PeLED devices were fabricated achieving a 99% high working ratio in a 62×47 array.[166]

5.2 Mask-free patterning

Among a series of patterning strategies, mask-free patterning methods provide a fast fabrication process and a noncontact strategy for AILHPs in display application. Benefitting from the printing technology in our daily lives, some groups develop inkjet printing to manufacture high-quality perovskite patterns, where liquid-phase AILHP materials are controlled to be transferred onto a target substrate. Pioneering studies were mainly focused on organic–inorganic hybrid perovskites,[167,168] and they suffered a lot from the intrinsic drawback of poor morphology induced by the "coffee ring".[169] To avoid the patterns showing "coffee ring", the perovskite seed array was first prepared by inkjet printing, and then was placed in a vapor atmosphere to grow $CsPbBr_3$ microplate arrays showing high luminescence.[170]

An alternative strategy to obtain highly efficient perovskite emitters through the inkjet printing methods is *in situ* formation of perovskite NCs by embedding liquid perovskite precursors in PDMS films, as shown in Fig. 6a. During the curing process at 80 °C, the space confinement of the liquid PDMS precursor can slow the nucleation and the crystal growth for the controllable fabrication of wafer-scale flexible perovskite fluorescent patterns working in an ambient environment.[171] Besides, some strategies are developed to improve the disadvantage of "coffee ring" in printing precursor inks. Through incorporating polyvinylpyrrolidone (PVP) into perovskite precursor solutions and adjusting the nozzle temperature, AILHP NCs with uniform size (~30 nm) distribution and smooth

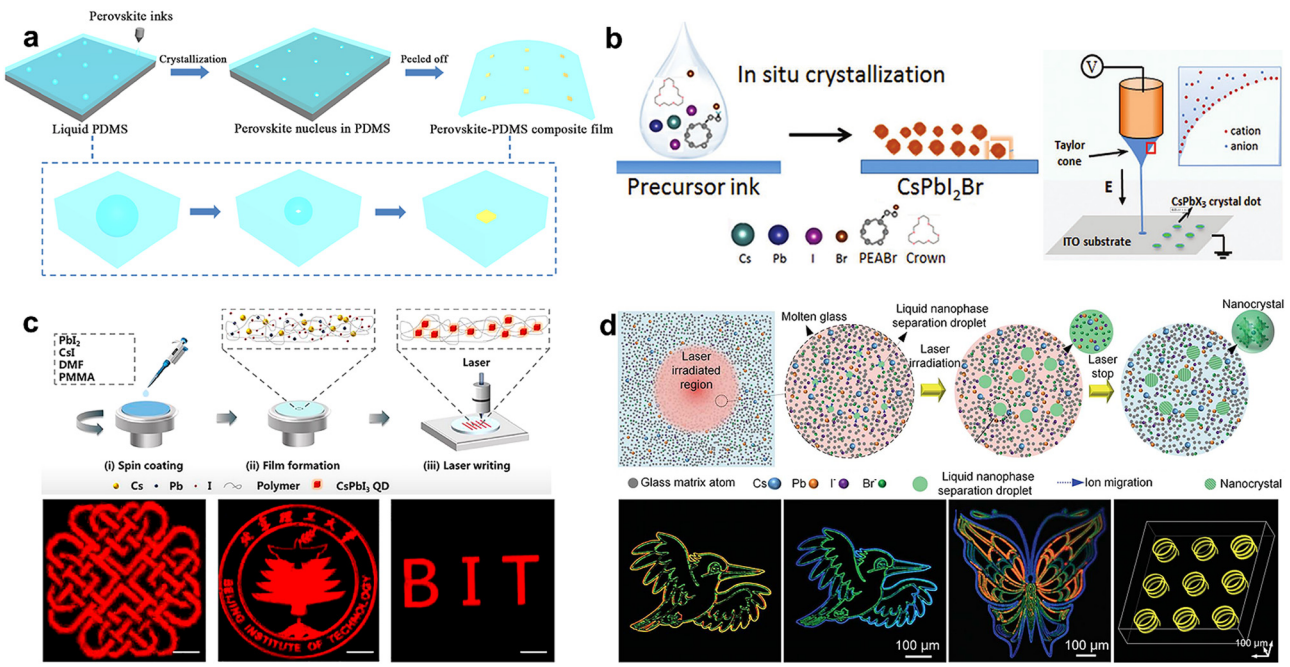

Fig. 6 Perovskite structures prepared by mask-free patterning. (a) Inkjet printing methods *via* embedding liquid perovskite precursors in PDMS films. Reprinted with permission from ref. 171. Copyright 2020, American Chemical Society. (b) E-jet printing with suitable additives for controllable morphology of perovskite structures. Reprinted with permission from ref. 177. Copyright 2019, Wiley-VCH. (c) Direct laser writing induced photothermal heating for chemical reactions of $CsPbI_3$. Reprinted with permission from ref. 181. Copyright 2021, American Chemical Society. (d) Ultrafast laser-induced liquid phase separation and ion migration for colorful patterns. Reprinted with permission from ref. 131. Copyright 2022, The American Association for the Advancement of Science.

Published on 29 March 2023. Downloaded by Yunnan University on 8/16/2025 4:33:01 AM.

morphology were obtained, where the increase of temperature of the nozzle as well as the precursor solutions had a positive effect on decreasing the viscosity of precursor ink.[172] If we focus on modifying the printing substrate, perovskite precursors in DMF or dimethyl sulfoxide (DMSO) were printed onto pre-heated polymer substrates, such as PMMA and polystyrene (PS), where the soluble properties of these polymer materials in DMF and DMSO solvents make the polymer substrates quickly dissolve or swell perovskite inks.[167] Recently, a tentative experiment was performed to effectively suppress the printed morphology of ''coffee ring'', by dispersing perovskite QDs with a high-boiling-point solvent of dodecane and a low-boiling-point one of toluene. The mechanism should be understood that the formation of appropriate Marangoni flow balances the capillary flow, resulting in the elimination of the ''coffee ring'' effect.[173]

The inkjet printing method has to face the barrier of depositing ultrahigh-resolution patterns, which is attributed to the difficulty in the generation of an ultrasmall volume of droplets with widely used thermal and piezoelectric printer nozzles.[174] Electrohydrodynamic jet (e-jet) printing fills the blanks in generating ultrasmall volume (*i.e.*, femtoliter) of droplets, which is assisted by applying an electric-field between the nozzle and the substrates.[175,176] The *in situ* formation of $CsPbX_3$ patterns with multiple-color emission and high resolution (pixel size of 5 μm) was achieved, where phenethylammonium bromide (PEABr) and 18-crown-6 were selected to control the morphology and suppress the phase segregation of the perovskite (Fig. 6b).[177] E-jet printing has its advantages in fabricating complex 3D microstructures, because the small volume of droplets allows the ink materials to crystallize directly without any further posttreatment.[178,179]

Laser is well known as a powerful tool for industrial manufacturing, and explored as a kind of noncontact fabrication method for perovskite patterning. When intense laser interacts with active materials, photothermal heating, direct ablation, and photochemical reaction are accompanied, which help to induce localized perovskite crystallization forming patterned perovskites in various mechanisms.[180] Fig. 6c shows an efficient and simple scheme of patterning QDs by direct laser writing based on a 405 nm nanosecond laser, where the patterning mechanism is based on photothermal heating induced chemical reactions of γ-phase $CsPbI_3$. The quantum yield of γ-$CsPbI_3$ QDs was detected up to 92% with a minimum line width down to 0.9 μm.[181] A focused continuous-wave laser (405 nm) could be also utilized to remove the surfactants around AILHP NCs. With laser scanning, the area exposed by laser irradiation remained, but the area with the surfactant (not exposed to laser) was easily washed away by the solvent.[182] Moreover, if the laser focus position was controlled at the solid–liquid interface, the huge transient energy of femtosecond (fs) laser can instantly reach the threshold of generating microbubbles of liquid. The bubbles exerted the Marangoni effect on the fluid thereby generating a circulating flow, and accumulated QDs in the fluid at the bottom. The subsequent drying of the liquid could cause QDs to be aggregated on the substrate resulting in complex patterning, including fluorescence microwires and photos.[183] The fabrication precision of the laser writing method is sensitively related to the position, the spot size, and the light intensity of the laser.[184]

Benefitting from the advantages of the focus-sensitive mechanism, 3D patterning can be conducted by laser printing. AILHP NCs in glass with tunable composition and bandgap were reversibly fabricated by ultrafast laser-induced liquid phase separation, where the migration of high mobility ions could be driven by a laser induced local thermal field, and the aggregation or the separation of nanophase from the glass matrix was also promoted by laser, as shown in Fig. 6d. The transparent dielectric materials of glass provide a solid platform for 3D reversible patterning of perovskite NCs, which hold great promise in future optical storage, micro-LEDs, and holographic displays.[131] The writing mechanism has been systematically investigated with respect to the laser intensity, the exposure time, and the moving speed of samples.[185] Even strong nonlinear optical properties were observed in QDs written in glass, and the erasing process could be completed by inducing a second irradiation at a certain laser fluence.[186] Interestingly, combining laser-writing perovskite patterns with moisture field modulation, the four-dimensional flexible instantaneous reading of time-resolved information encryption is endowed with the ability to control the fs-laser exposure time and the fluidity of moisture.[187]

6. Advanced display devices

6.1 Light-emitting devices with color conversion layers

In the early stage, AILHP NCs have been utilized as color-conversion luminescent materials for blue-LED or UV-LED chip-driven WLEDs. When AILHP NCs are integrated as the color conversion layer on the top of the blue-LED chip, they need to suffer from the high working temperature even higher than 150 °C, and a polymer such as PMMA is used to disperse AILHP NCs preventing the temperature caused ion-exchange. WLEDs were assembled by combining blue-LED chips and red/green $CsPbX_3$ QD/PMMA composites, and their correlated color temperature (CCT) could be adjusted by changing the ratio of red and green QDs ranging from 2500 to 11 500 K.[75] Some works proved that PMMA could lead to the degradation of AILHP NCs, hence ethyl cellulose (EC)-based $CsPb(Br_{0.4}I_{0.6})_3$ QDs were utilized to make warm white light, showing a high LE of 46.45 lm W^{-1} and a CRI of 90.3 (Fig. 7a).[188] Similarly, $CsPbBr_3$ NCs with a thick polymer coating of maleic anhydride-*alt*-1-octadecene (PMAO) were prepared in the combination of a commercial red-emitting phosphor for a warm WLED (Fig. 7b).[189] Besides, there is a common strategy to build broadband-emission WLEDs, by blending AILHPs with other materials (like $C1_4H_{10}$). This type of WLED showed a CRI of 90 and a tunable CCT from 2911 to 8572 K.[190]

The direct contact of the NC layer and blue-LED chip could lead to the thermal quenching and the photodegradation of NCs. To avoid this disadvantage, QD enhancement films

 This journal is © The Royal Society of Chemistry 2023

Published on 29 March 2023. Downloaded by Yunnan University on 8/16/2025 4:33:01 AM.

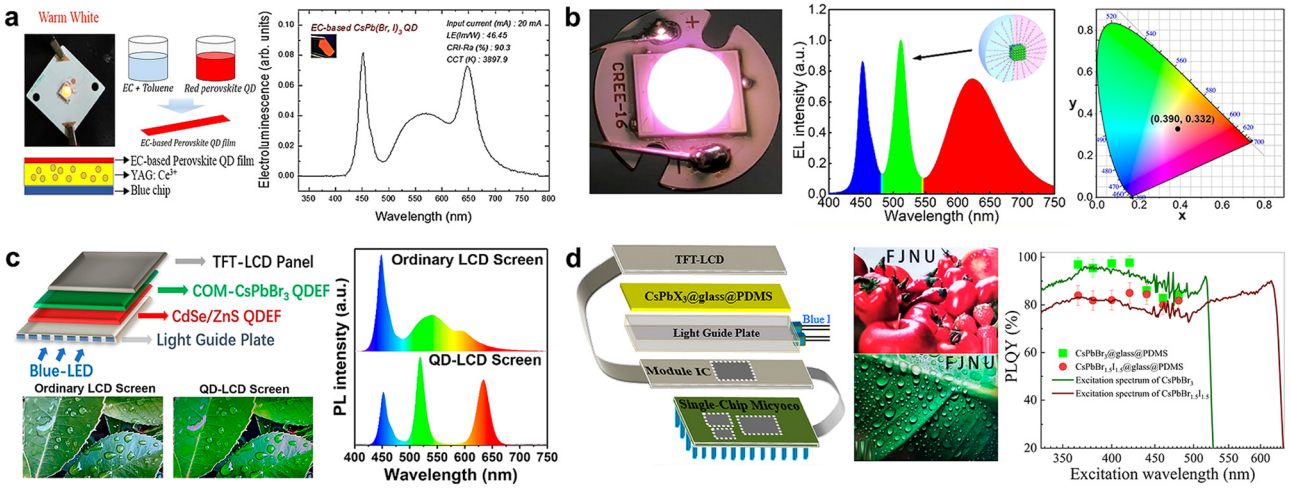

Fig. 7 Light-emitting devices with perovskite color conversion layers. (a) A warm WLED with a color conversion layer of EC-based $CsPb(Br_{0.4}I_{0.6})_3$ QDs. Reprinted with permission from ref. 188. Copyright 2017, Elsevier. (b) Ultrastable WLEDs based on $CsPbBr_3$ NCs coated with a thick PMAO. Reprinted with permission from ref. 189. Copyright 2019, American Chemical Society. (c) Schematic of the perovskite-based device structure and their display characteristics. Reprinted with permission from ref. 195. Copyright 2022, American Chemical Society. (d) Schematic illustration of the LCD device structure and their display effect in red and green. Reprinted with permission from ref. 71. Copyright 2021, American Chemical Society.

(QDEFs) have already been mass produced by several TV manufacturers and research groups, where large-area and uniform QD films are placed over the entire display.[191–193] However, there is still a need to develop cost-effective and scalable manufacturing techniques for AILHP enhancement films.[194] As shown in Fig. 7c, organic semiconducting molecules were introduced as the capping ligands for stabilizing $CsPbBr_3$ QDEF films, which presented an extremely high stability in QD-enhanced LCD prototypes with harsh commercial accelerated operational tests.[195] The QDEF of $CsPbBr_3$ with strong dipole–dipole interaction between the C–F bonds of fluoroelastomers show excellent self-healing ability with micron- and centimeter-scale cracks. These films enabled practical applications in flexible WLEDs exhibiting vivid pictures with high saturations for object colors.[72] Improved $CsPbBrI_2$ QDs embedded into PMMA were deposited on the upper surface of YAG:Ce^{3+} based WLEDs to make up the missing part of the red spectrum of YAG:Ce^{3+} based WLEDs. The fabricated WLED exhibited a luminescence efficiency (LE) of 58 lm W^{-1}, a CCT of 5907 K, and a color rending index (CRI) of 90.[196] The low-temperature molten salt (KNO_3–$NaNO_3$–KBr) synthesis of $CsPbBr_3$ NCs were further enclosed in a UV-curable acrylate polymer for WLEDs, which emitted white light with color coordinates of (0.2985, 0.3076) and a CCT of 7692 K.[197]

The AILHP QDEF film can also be fabricated on an inorganic glass matrix, which not only protects the QDs from external environments, but also effectively blocks the agglomeration and color segregation. Indeed, ~100% PLQY of green $CsPbBr_3$@ glass and ~80% PLQY of red $CsPbBr_{1.5}I_{1.5}$@glass films were successfully achieved, which were tested successfully as the backlight in LCDs showing a much wider color gamut (Fig. 7d).[71] In another work, the yellow $CsPbBr_{1.8}I_{1.2}$ QDs-epoxy resin film was prepared on a glass, and it was integrated with blue gallium nitride (GaN) micro-LEDs (80 μm × 80 μm) forming a white light system. For the application of visible light communication, a high modulation bandwidth of 85 MHz and a real-time data rate of 300 Mbps were recorded.[198]

Recently, with the rapid growing field of augmented and mixed reality (AR/VR), near-eye display and wearable display devices appearing as the new-generation display technologies have attracted substantial interest, which require sub-10 μm pixels with short response times (~ns) and high optical contrast (>1 : 10 000) for flicker-free imaging.[199,200] Although, LCDs and micro-OLEDs dominate the current market, their limited display intensity and large device volume cannot provide comfortable user's experience in outdoor and sports scenes.[201,202] Recent advances in complementary metal–oxide–semiconductor (CMOS)-integrated GaN LEDs open up the doors for the miniaturization of individual pixels down to a few micrometers. It is a consensus in the display industry that the realization of full-color micro-LED displays based on GaN-chips cannot be separated from the help of color conversion of QDs.

By patterning traditional QDs as the color conversion layer on 5 μm-scale GaN micro-LED arrays, Fig. 8a presents a recent work showing the ability to fabricate emissive-type LEDs with 1270 PPI ultrahigh resolution.[203] The results came from several technical integrations, including wafer-scale GaN/Si epilayer transfer, high-precision aligned fabrication with CMOS integration, and dry patterning of full-color QDs. Although perovskite QDs were not adopted in this work, it indeed guided the road and made significant progress in near-eye display prototype suitable for forthcoming novel applications. As the research on AILHP QDs coupled micro-LEDs is the pioneer in the research field, the reported results are quite less. Only in one work based on microfluidic technology, AILHP QD color conversion layers with a full-color pixel size of 200 × 200 μm and a sub-pixel size of 140 × 50 μm were achieved and integrated on a blue micro-LED array, as shown in Fig. 8b, which performed as a wide color gamut of 131% (National Television Systems Committee standard).[204] In the last two years, our group developed some

Published on 29 March 2023. Downloaded by Yunnan University on 8/16/2025 4:33:01 AM.

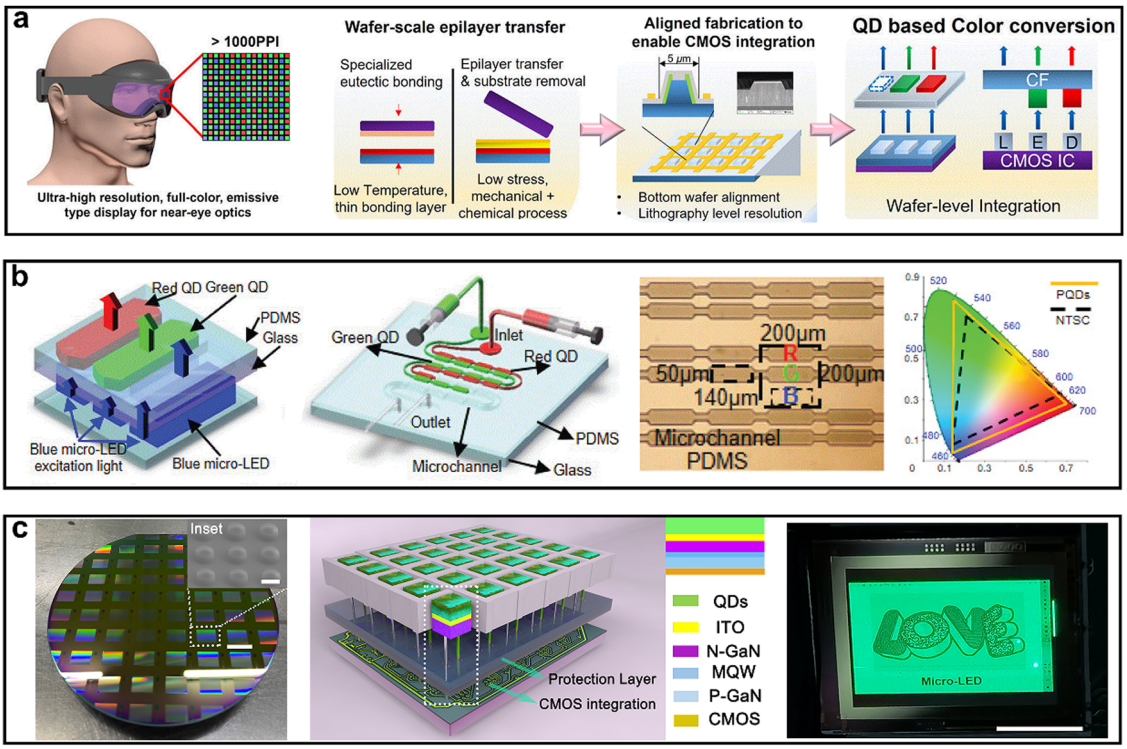

Fig. 8 Micro-LEDs consisting of QD color conversion layers on a GaN LED chip. (a) Patterning traditional QDs on a 5 μm-scale GaN micro-LED for near-eye display prototype. Reprinted with permission from ref. 203. Copyright 2022, Springer Nature. (b) Microfluidics-induced QD color conversion layers for full-color micro-LED display. Reprinted with permission from ref. 204. Copyright 2021, AIP Publishing. (c) PMMA mixing green QDs patterned on GaN micro-LEDs (scale bar is 8 μm) for microscreen display with 2 K resolution.

micro-LED techniques realizing the monolithic integration of a 4-inch Si-based GaN micro-LED of 7.5 μm pixels. Fig. 8c shows the wafer-scale micro-screen with 1920 × 1080 resolution. From the schematic and the cross-sectional views of the device, GaN micro-LED arrays were overlapped by green $CsPbBr_3$ QD color conversion layers on the top, and were integrated with CMOS circuits at the bottom for dynamic pattern displays, showing the picture of "love". Although detailed results have not been reported yet, the effort devoted into the wafer-scale patterning of AILHP QDs on GaN micro-LEDs was worthy for future advanced displays.

6.2 Electroluminescence devices with self-luminous layers

AILHP NCs are naturally compatible with flexible or bendable display devices, which have aroused worldwide concerns in the application of PeLEDs for decades. As the self-luminous layer of an EL device, the photon emission is generated by the recombination of electrons and holes, which are hooped or injected by the neighboring electron and hole transfer layers, respectively. The performances of PeLEDs are decided by the stability of NCs, the quality of the NC film, and the device structure. Numerous studies have been devoted to enhancing the device performance through composition design, surface engineering, and device structure modification. The first PeLED was fabricated with organic $MAPbBr_3$ QDs in 2014.[205] In the last three years, PeLEDs based on AILHP NCs have been reported successively. One possible strategy is ion doping, where Ni^{2+} ions were incorporated into $CsPbCl_xBr_{3-x}$ QDs during the process of supersaturated recrystallization (Fig. 9a). By modulating the ratio of Cl/Br elements, a maximum luminance of efficient blue PeLEDs was recorded as 612 cd $m^{-}2$ and 2.4% EQE.[206] A similar work reported that red PeLEDs based on Ni^{2+} (3.3 mol%): $CsPbI_3$ NCs exhibit an EQE of ~7%.[207]

As another effective strategy, surface ligand engineering has been widely reported in enhancing the device performance of PeLEDs.[208] On the one hand, the surface capping ligands can fill in the surface defects improving the stability of NCs, and on the other hand, they also perform as an insulating layer hindering the charge transfer. Therefore, the rational design of surface ligand modification can optimize the performance enhancement of PeLEDs.[12] Usually, the long-chain ligands should be replaced with short-chain ligands to enhance the LED performance.[209] A facile ligand-exchange method using amino acids was demonstrated to reduce long chain ligands on $CsPbI_3$ QDs. Owing to the passivation of extra sulfur ligands, the PeLED achieved an EQE of 18.0% and a T_{50} of 87 min (Fig. 9b).[210] Resurfacing NCs with inorganic ligands held the promise in realizing α-phase $CsPbI_3$ at room temperature. KI-exchanged $CsPbI_3$ QD films were reported presenting superior phase stability and increased thermal transport, which were further applied in PeLEDs exhibiting a maximum EQE of 23%.[211] Another work showed that a bifunctional molecule of trichloro(1*H*,1*H*,2*H*,2*H*-tridecafluoro-*n*-octyl)silane (PFTS) was employed for the synthesis of high-quality $CsPb(Br/Cl)_3$ NCs,

 This journal is © The Royal Society of Chemistry 2023

Published on 29 March 2023. Downloaded by Yunnan University on 8/16/2025 4:33:01 AM.

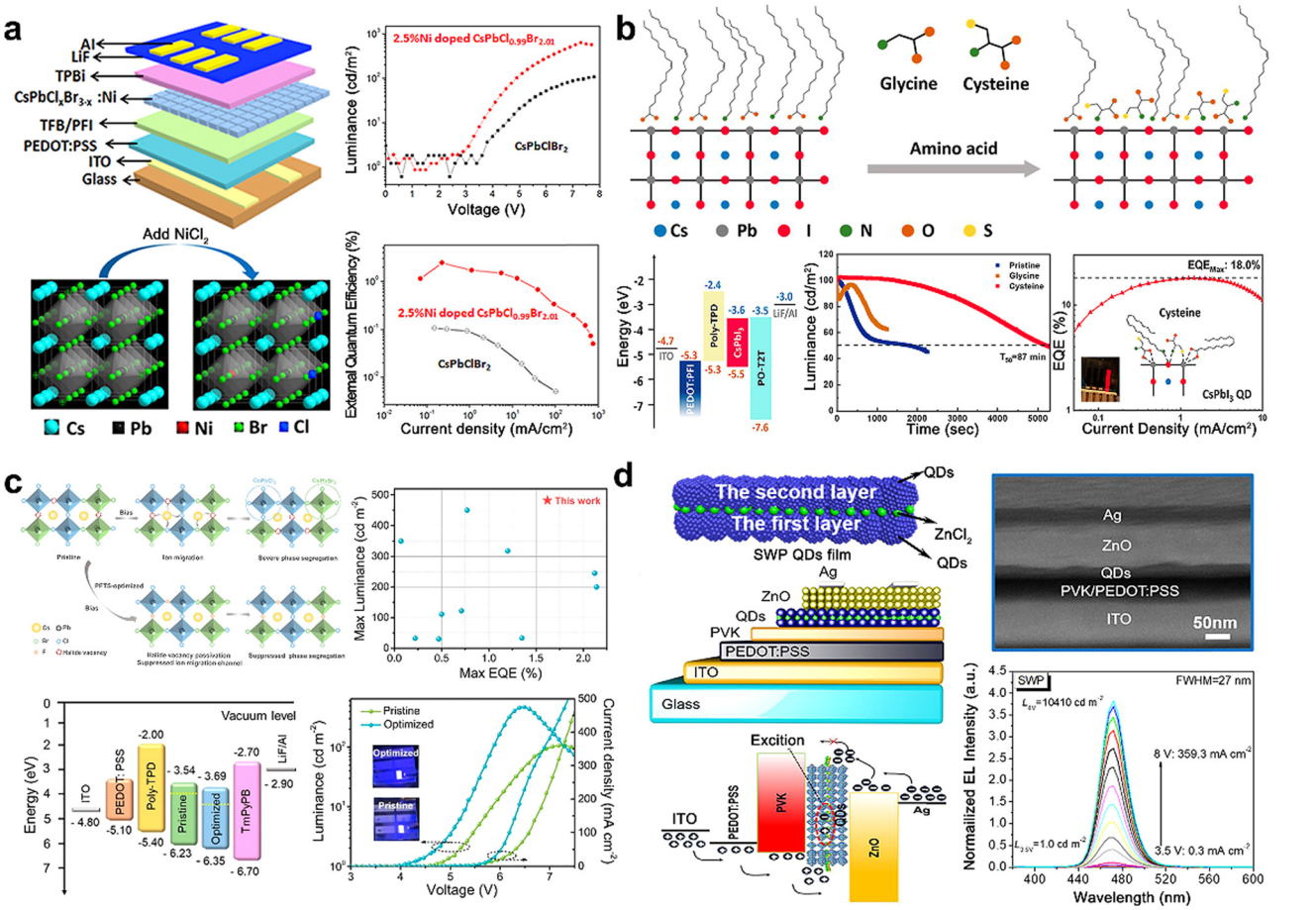

Fig. 9 Performances of PeLEDs using AILHP QDs as emitters. (a) PeLED structure and performance based on 2.5% Ni^{2+}-doped $CsPbCl_{0.99}Br_{2.01}$ QDs. Reprinted with permission from ref. 206. Copyright 2020, American Chemical Society. (b) Stability and EQE measurements of cysteine-exchanged $CsPbI_3$ QD LEDs. Reprinted with permission from ref. 210. Copyright 2023, American Chemical Society. (c) Working mechanism of PFTS optimization to achieve stable device characteristics. Reprinted with permission from ref. 212. Copyright 2022, American Chemical Society. (d) Device structure and EL spectra of the PeLEDs based on a novel structure sandwich panel (SWP) of QD films. Reprinted with permission from ref. 213. Copyright 2022, Elsevier.

where Cl^- ions worked as the Cl-precursors, and F^- ions helped to passivate the surface. At a wavelength of 461 nm, the optimized device reached an EQE of 1.62% and a luminance of 482 cd m^{-2} (Fig. 9c).[212]

The high-efficiency light emission needs balanced injection and uniform spatial distribution of electrons and holes injected from individual layers. Usually, the carrier mobility of the electron transport layer is $\sim 10^{-3}$–10^{-4} cm^2 V^{-1} s^{-1}, which is much higher than that of the hole transport layer ($\sim 10^{-4}$–10^{-6} cm^2 V^{-1} s^{-1}). By inserting a barrier layer of $ZnCl_2$ (Fig. 9d), recombination zone was changed away from the charge carrier accumulation at the interface of the emissive layer and hole transfer layer, which reduced the interfacial exciton quenching and Auger recombination creating a ultra-high brightness blue PeLED (>10 000 cd m^{-2}).[213] Besides, the core–shell structure provided a natural protective layer for stable NCs in high performance PeLEDs. A novel structure of perovskite NC arrays embedded in porous alumina membranes was prepared *via* a close-spaced vapor reaction. The uniform structure could be successfully grown on an Al sphere with a diameter of 1.5 cm. The EQE and luminance of this curved PeLED were recorded as 8.76% and 1300 cd m^{-2}, respectively.[214] Another work strengthened a unique method to simultaneously prepare mixed $CsPbBr_3$ QDs and Cs_4PbBr_6 NCs, and their PeLEDs have an EQE of 4.65% at 480 nm.[215]

Currently, the toxicity of lead-based perovskite QDs becomes an enormous obstacle lying on the way of commercialization for PeLEDs. Notably, it has been widely reported that lead elements can be replaced by other metals, such as Sn, Ge, Bi, and In. Generally, the tin-based perovskite is considered to be one of the most promising candidates, which has an elevated optical absorption coefficient and a narrowed optical band gap. Besides, the cooperation of the tin component can fill in the blank of near-infrared emission of PeLEDs, which boosts their applications in night vision cameras, information recognition, communication and biomedical instruments.[216,217] But they still face great challenges in high-performance light-emitting properties, which is due to the unfavorable characteristics of Sn^{2+} oxidation and high hole concentration. In 2021, the EQE efficiency of $CsSnI_3$ PeLEDs was only recorded as 5.4%.[218] Recently, researchers divert attention into other elements with a similar electrical structure and ionic radius, such as Bi^{3+}, Sb^{3+}

Published on 29 March 2023. Downloaded by Yunnan University on 8/16/2025 4:33:01 AM.

Table 1 Summary of light-emitting devices using ALLHP-NCs as color conversion layers

Material	Method	PL/FWHM (nm)	PLQY (%)	CRI (Ra)	CCT (K)	Rec. 2020	Stability	Year	Ref.
Mesoporous-$CsPbBr_3$/SDDA	Three-step treatment	523/23	71	—	—	~76[a]	71%PLQY (25–100 °C)	2016	26
$CsPb(Br_{0.75},Cl_{0.25})_3$	Hot-injection method	499/18	63	96	6500	~108[a]	—	2016	29
$CsPbBr_3$/silica	Hot-injection method	522/22	85	—	—	~90[a]	Stable (10 h, 61.2 lm W^{-1})	2016	146
$CsPbBrI_2$	Hot-injection method	656/—	65	90	5907	—	—	2016	196
EC-$CsPb(BrI)_3$	Hot-injection method	641/32	34.2	90.3	3897.9	—	65%PLQY (150 h, water)	2017	188
$CsPbCl_{0.5}Br_{2.5}$	Hot-injection method	511/20.4	61	—	—	100.4	85%PL (7 day, ambient atmosphere)	2018	23
Mn^{2+}-doped $CsPbCl_3$	Solvothermal synthesis method	600/100	64.2	80	5196	—	Stable (298–335 K)	2018	88
$CsPbBr_3$ NCs/PMMA	Seed-mediated solvothermal synthesis method	514/18	50	—	—	~100[a]	—	2018	94
$CsPbBr_3/SiO_2$	Water-triggered transformation process and a sol–gel method	517/18	80	63	—	~103[a]	98%PL (10 h, UV)	2018	158
$CsPb(Br/I)_3$@anthracene	Hot-injection method	White	41.9	72–90	2911–8572	—	50%PL (20–100 °C)	2018	190
Mn^{2+} doped $CsPb(Cl_{0.6}Br_{0.4})_3$	Hot-injection method	450/—	65		4000	—	—	2019	86
$CsPbBr_3$-PQDs/MPMs@SiO_2	Hydrolysis encapsulation method	518/23	84	—	—	—	88%PL (5 day, water)	2019	149
$CsPbMn(BrCl)_3$@SiO_2	Reverse microemulsion method	446/—	50.5	87–91	3857–5934	—	90%PL (1 h, 100 °C)	2019	152
$CsPbBr_3$	Inkjet-printing and UV-curing method	514/19	96	—	—	—	93%PL (90 day, ambient atmosphere)	2019	169
PMAO-$CsPbBr_3$	Postsynthetic method	512/—	88.8	—	3320	—	60%PL (24 h, water)	2019	189
$CsPb(Cl_{0.5}/Br_{0.5})_3$ PNCs@SiO_2/PMMA	Hot-injection method	460/22	9.7	84.7	4825	98.56	76.2%PL (25 day, water)	2020	63
γ-$Rb_{0.5}Cs_{0.5}PbI_3$	*In situ* fabrication	642/—	91	—	—	97	95%PL (1000 h, 60 °C/90%RH)	2021	193
$CsPbBr_3$/mesoporous-SiO_2	Molten-salts-based method	520/21.5	90	—	7692	—	95%PL (30 day, water)	2021	197
$CsPbBr_3$	Microfluidic method	517/17.3	90	—	—	~98[a]	—	2021	204
BSZ-2Ti	Self-crystallization method	517/—	41.2	—	6216	93.15	80%PL (20 day, water)	2022	64
$CsPbBr_3$@AGs	Hot-injection method	518/—	71	94.9	5477	~95[a]	~90%PL (47 day, UV)	2022	69
$CsPbBr_3$@glass@PDMS	*In situ* precipitation method	514/16	95	—	—	~75[a]	85%PL (500 h, 85 °C/85%RH)	2022	70
$CsPbBr_3$ QPFs	Room temperature precipitation method	525/25	96.1	—	—	96	97%PL (100 cycle, tensile)	2022	72
$CsPbBr_3$ PNCs/PVDF	Low-temperature liquid phase method	520/~20	—	—	—	~80[a]	80%PL (84 h, UV)	2022	194
COM-$CsPbBr_3$	Solvothermal method	518/16	82	—	—	93	Stable (96 day, 85 °C/85%RH)	2022	195

[a] The Rec.2020 is calculated at 0.74 NTSC.RH = relative humidity.

and In^+/In^{3+}. In the lattice conformations described by $A_2B(I)B(III)X_6$, $A_3B(III)X_9$, and $A_2B(IV)X_6$, a family of double perovskites are created. For example, $Cs_2AgInCl_6$ alloyed with 40% Na^+ and 0.04% Bi^{3+} doping emitted warm white light with ~86% PLQY, and worked for 1000 hours without obvious PL loss.[219] The further development of lead-free PeLEDs is worth pursuing, which indeed meet the demand of source-saving and environment-friendly development.

7. Conclusions and perspectives

In the recent Consumer Electronics Show 2023, many companies exhibited their refreshing and innovative display/lighting technologies, providing an avenue for the future development of perovskite-based display devices. For examples, Samsung and LG companies exposed a series of large-scale, flexible, self-lighting display devices.[220–222] Macroblock company expanded the application of LEDs for head-up displays in cars, which show high precision and high brightness characteristics in complex outdoor environments.[223] Carmaker of Audi presented the digital car headlight for interactive experiences of human-car-nature by smart lighting and imaging.[224] Meeting the rising demand of consumer electronics based on advanced display devices, AILHP NCs have been seen as great potential materials for next-generation candidates in wide color gamut backlighting and high resolution full-color displays.

In this work, focusing on the potential combination and integration of AILHP NCs in display devices, the synthesis method, the stability optimization, the working mechanism, and the device structure are summarized, and their recent remarkable progress is concluded and reviewed. In contrast to conventional semiconductor QDs or organic perovskite QDs, AILHP NCs have considerable merits such as facile synthesis, high PLQYs, optimized stability and tunable emission, due to their unique intrinsic structural and optoelectronic characteristics. Although they face common issues of structural or spectral instability when exposed to the air or the moisture environment, strategies such as ligand engineering, ion exchange and insulator coating have been explored to improve the above-mentioned serious problems.

 This journal is © The Royal Society of Chemistry 2023

Published on 29 March 2023. Downloaded by Yunnan University on 8/16/2025 4:33:01 AM.

Table 2 Summary of EL devices using AILHP-NCs as self-luminous layers

Material	Method	EL/FWHM (nm)	EQE_{max} (%)	L_{max} (cd m^{-2})	CE (cd A^{-1})	CIE	Device stability	Year	Ref.
$CsPbBr_3$	Hot-injection method	512/20	6.27	15 185	13.3	—	—	2017	12
$CsPbBr_3$-$MnBr_2$	Organic–inorganic hybrid ligand method	520/—	15.6	100 080	60.6	—	T_{50} (136 min, 0.6 mA cm^{-2})	2018	19
$CsPbBr_3$/MABr quasi-core/shell structure	One-step deposition method	525/20	20.3	14 000	78	(0.18, 0.75)	T_{50} (100 h, 100 cd m^{-2})	2018	46
$Cs_xFA_{1-x}PbBr_3$	Solution-based approach	483/26	9.5	54	12	(0.094, 0.184)	T_{50} (250 s, 100 cd m^{-2})	2019	48
$CsPbBr_3$	Water-triggered transformation method	520/18	8.2	980	25.7	—	—	2019	82
$CsPbBr_3$	Room temperature method	520/18	21.63	4064	81.4	(0.17, 0.74)	T_{50} (180.1 h, 100 cd m^{-2})	2020	17
$(PEABr)_{0.4}CsPbBr_3$	Large-area photolithographic method	513/19	1.24	13 043	3.85	—	—	2020	160
$CsPbBr_3$	PDMS template confined solution growth method	530/14	—	—	—	—	T_{50} (60 min, 5 V/1.5 mA)	2020	166
$CsPbCl_{0.99}Br_{2.01}$	The room-temperature super-saturatedrecrystallization synthetic method	470/—	2.4	612	—	—	—	2020	206
A-$CsPbBr_3$@SiO_2	Hot-injection method	515/20	0.12	3200	5.3	—	T_{50} (43 min, 100 cd m^{-2})	2021	151
Ni^{2+}(3.3 mol%): $CsPbI_3$	Hot-injection method	690/—	7	830	1.2	—	T_{50} (1900 s, 5 V)	2021	207
$CsPbI_3$	Inorganic ligand exchange	640/31	23.0	200	—	—	T_{50} (10 h, 200 cd m^{-2})	2021	211
$CsPbI_3$	Passivation strategy	650/32	7.3	972	10.3	(0.71, 0.29)	—	2022	27
$CsPbBr_3$-PAN	Micro- and capillary-molding processes	517/18	12.8	10 737	52.3	—	T_{50} (993 s, 10737 cd m^{-2})	2022	28
$CsPbBr_3$	Ternary-solvent-ink strategy	517/18	8.54	43 883.39	7.7	(0.09, 0.74)	T_{50} (63.84 min, 100 cd m^{-2})	2022	66
$CsPbBr_3$	Microemulsion method	460/17	2.01	128	1.13	(0.138, 0.046)	T_{50} (45 day, 100 cd m^{-2})	2022	68
$CsPb(Cl/Br)_3$	Hot-injection method	508/17	2.16	>1000		(0.07, 0.70)	—	2022	81
t-PeQD-Br	Hot-injection method	515/19	4.65	9084.9	16.02	—	—	2022	209
Cysteine-treated $CsPbI_3$	Ligand-exchange method	653/~35	18.0	250	—	(0.714, 0.283)	T_{50} (87 min, 100 cd m^{-2})	2022	210
$CsPb(Br/Cl)_3$	Hot-injection method	461/14.6	1.62	482	—	—	—	2022	212
$CsPbI_3$	Hot-injection method	469/27	5.0	10 410	—	(0.13, 0.11)	T_{50} (59 h, 100 cd m^{-2})	2022	213
$CsPbBr_3$-Cs_4PbBr_6	*In situ* surface reconstruction method	480/—	4.65	23	5.1	—	—	2022	215

Besides, there is a big step towards the application of pixel-displayed light-emitting devices, that is the full-color patterning of NCs, where traditional photolithography, e-beam lithography and nano-imprinting, as well as new-type inkjet or e-jet printing are introduced to fabricate colorful pixel arrays and large-scale pictures. Finally, recent progress in advanced display devices based on AILHP NCs are systematically reviewed, among WLEDs, QLEDs, QD-LEDs, and micro-LEDs, which can be concluded into four device models. We are intended to highlight the important role of AILHP NCs in creating advanced display devices as color conversion layers or self-luminous layers. Tables 1 and 2 conclude the main parameters of AILHPs working in two kinds of display devices mentioned in this review.

However, considering the requirement in industrial manufacturing, three main obstacles continue to restrict their practical applications. First is the large-scale and batch manufacturing technique. Though the synthesis processes of NCs are simple and easy to industrialize, and they show great compatibility of solution processing, involving spin-coating, blade-coating, roll-to-roll, almost all reports were still conducted in labs. With the detailed consideration of earth-abundant precursors and cheap manufacture costs, taking PeLED as an example, the cost is estimated as 2533 lm per $, which is much higher than those of any other lighting technologies.[225] More efforts are needed to be devoted in the process of magnifying yields and saving costs, and the roadmap of the production line process is urgent to be simplified and optimized. Besides, in the devices of PeLEDs and backlight, the light-emitting performance of large-area devices still lags behind the corresponding small-area devices, which can be attributed to microscopic defects and nonradiative electronic traps.[226] Drawing lessons from the experience accumulation of solution-processing manufacturing techniques in perovskite photovoltaic engineering,[227,228] we believe these could provide an important impetus in the development of display devices based on AILHP NCs.

Second is the structural and emission stability. In the current state, the device lifetime of monochromatic light-emitting devices based on AILHP NCs varies from less than an hour to hundreds of hours, which is much far behind the commercial goal of tens of thousands of hours. AILHP NCs are a class of ionic crystals suffering from the weak fairly ionic bonding and low crystal lattice energy. When AILHP NCs are exposed to high humidity, high temperature or strong light, all kinds of perovskite materials show decomposition or an emission degrading phenomenon in different degrees.[229] In particular, intense light can break the weaker bonds in perovskites leading to halogen ion migration or conversion of possible

Published on 29 March 2023. Downloaded by Yunnan University on 8/16/2025 4:33:01 AM.

oxygen into highly reactive superoxides. When AILHP NCs are integrated into devices, several interfaces are created, and the unflatness of the layer surface or the interface stress force disturbed by temperature has a direct impact on the decrease of device performance.[230] In the short-term, devices with color conversion layers are likely to be the first and fastest towards commercialization, but for a long-term consideration, breaking through the barrier of performance stability of EL devices is quite necessary, which may set off a revolution of the perovskite light-emitting device.

Third is the environment protection. It is inevitable for optoelectronic devices generating metal or non-biodegradable pollutants to the natural environment, and heavy-metal-based substances in electronic devices are strictly limited by many countries and institutions. Most AILHP NCs contain elements of lead family, which increases the risks in bringing danger to the human nervous, cardiovascular, skeletal, reproductive, and immune systems.[231] Although the current limit for lead (1000 ppm by weight) is much less than that of cadmium (100 ppm by weight), current recycling policies for lead in consumer electronics are working well.[232] The development of lead-free all-inorganic perovskite NCs and their devices is necessary, which also needs to be encouraged.

In summary, we believe that AILHP NCs with their superior optical characteristics and flexible preparation methods will lead to the application of advanced display applications in the near future.

Conflicts of interest

There are no conflicts to declare.

Acknowledgements

This work is supported by the National Natural Science Foundation of China (No. 62275076, 92163135, 52221001, U19A2090 and 62090035), the Key Program of the Hunan Provincial Science and Technology Department (2019XK2001 and 2020XK2001), and the Shanghai Pilot Program for Basic Research (22JC1403200). This work is also supported by the Open Project Program of Wuhan National Laboratory for Optoelectronics (2022WNLOKF003).

References

1 J. A. Castellano, *SID Symposium Digest of Technical Papers*, 1999, **30**, 356–359.
2 S. S. Kim, B. H. Berkeley, K.-H. Kim and J. K. Song, *J. SID*, 2004, **12**, 353–359.
3 S.-J. Kang, H.-C. Do and B.-G. Cho, *IEEE Trans. Consumer Electronics*, 2005, **51**, 204–209.
4 A. Jovicic, J. Li and R. Tom, *IEEE Commun. Mag.*, 2013, **51**, 26–32.
5 A. Salehi, X. Fu, D. H. Shin and F. So, *Adv. Funct. Mater.*, 2019, **29**, 1808803.
6 R. Pode, *Renew. Sust. Energ. Rev.*, 2020, **133**, 110043.
7 S. C. Xia, R. C. Kwong, V. I. Adamovich, M. S. Weaver and J. J. Brown, Proceedings of the 45th Annual 2007 IEEE International Reliability Physics Symposium, 2007, 253-257.
8 J.-H. Lee, C.-H. Chen, P.-H. Lee, H.-Y. Lin, M.-K. Leung, T.-L. Chiu and C.-F. Lin, *J. Mater. Chem. C*, 2019, **7**, 5874–5888.
9 B. R. Sutherland and E. H. Sargent, *Nat. Photon.*, 2016, **10**, 295–302.
10 Q. A. Akkerman, G. Raino, M. V. Kovalenko and L. Manna, *Nat. Mater.*, 2018, **17**, 394–405.
11 X. K. Liu, W. Xu, S. Bai, Y. Jin, J. Wang, R. H. Friend and F. Gao, *Nat. Mater.*, 2021, **20**, 10–21.
12 J. Li, L. Xu, T. Wang, J. Song, J. Chen, J. Xue, Y. Dong, B. Cai, Q. Shan, B. Han and H. Zeng, *Adv. Mater.*, 2017, **29**, 1603885.
13 G. Nedelcu, L. Protesescu, S. Yakunin, M. I. Bodnarchuk, M. J. Grotevent and M. V. Kovalenko, *Nano Lett.*, 2015, **15**, 5635–5640.
14 L. Protesescu, S. Yakunin, M. I. Bodnarchuk, F. Krieg, R. Caputo, C. H. Hendon, R. X. Yang, A. Walsh and M. V. Kovalenko, *Nano Lett.*, 2015, **15**, 3692–3696.
15 F. Liu, Y. Zhang, C. Ding, S. Kobayashi, T. Izuishi, N. Nakazawa, T. Toyoda, T. Ohta, S. Hayase, T. Minemoto, K. Yoshino, S. Dai and Q. Shen, *ACS Nano*, 2017, **11**, 10373–10383.
16 Q. Shan, J. Song, Y. Zou, J. Li, L. Xu, J. Xue, Y. Dong, B. Han, J. Chen and H. Zeng, *Small*, 2017, **13**, 1701770.
17 T. Fang, T. Wang, X. Li, Y. Dong, S. Bai and J. Song, *Sci. Bull.*, 2021, **66**, 36–43.
18 G. J. Supran, Y. Shirasaki, K. W. Song, J.-M. Caruge, P. T. Kazlas, S. Coe-Sullivan, T. L. Andrew, M. G. Bawendi and V. Bulović, *MRS Bull.*, 2013, **38**, 703–711.
19 J. Song, T. Fang, J. Li, L. Xu, F. Zhang, B. Han, Q. Shan and H. Zeng, *Adv. Mater.*, 2018, **30**, 1805409.
20 Y. Lee, D. S. Kim, S. W. Jin, H. Lee, Y. R. Jeong, I. You, G. Zi and J. S. Ha, *Chem. Eng. J.*, 2022, **427**, 130858.
21 W. Su and F. Yuan, *Matter*, 2022, **5**, 2464–2466.
22 A. Hong, J. Kim and J. Kwak, *Adv. Optical Mater.*, 2020, **8**, 2001051.
23 Y. H. Ko, M. Jalalah, S. J. Lee and J. G. Park, *Sci. Rep.*, 2018, **8**, 1–7.
24 Y. Yin, Z. Hu, M. U. Ali, M. Duan, L. Gao, M. Liu, W. Peng, J. Geng, S. Pan, Y. Wu, J. Hou, J. Fan, D. Li, X. Zhang and H. Meng, *Adv. Mater. Technol.*, 2020, **5**, 2000251.
25 A. K. Srivastava, W. Zhang, J. Schneider, J. E. Halpert and A. L. Rogach, *Adv. Sci.*, 2019, **6**, 1901345.
26 X. Zhang, H.-C. Wang, A.-C. Tang, S.-Y. Lin, H.-C. Tong, C.-Y. Chen, Y.-C. Lee, T.-L. Tsai and R.-S. Liu, *Chem. Mater.*, 2016, **28**, 8493–8497.
27 G. Lee, S. Y. Lee, S. Park, S. H. Jang, H.-K. Park, I. Choi, J. Park and J. Choi, *J. Mater. Res. Technol.*, 2022, **18**, 4145–4155.
28 H. J. An, M. S. Kim and J.-M. Myoung, *Chem. Eng. J.*, 2023, **453**, 139927.
29 H. C. Yoon, H. Kang, S. Lee, J. H. Oh, H. Yang and Y. R. Do, *ACS Appl. Mater. Inter.*, 2016, **8**, 18189–18200.

 This journal is © The Royal Society of Chemistry 2023

Published on 29 March 2023. Downloaded by Yunnan University on 8/16/2025 4:33:01 AM.

30 W. Wu, S. Wang, C. Zhong, M. Piao and Y. Zhao, *IEEE Access*, 2019, **7**, 32030–32036.
31 S. Srivastava, K. E. Lee, E. A. Fitzgerald, S. J. Pennycook and S. Gradecak, *ACS Appl. Mater. Inter.*, 2022, **14**, 48995–49002.
32 J. K. Sheu, S. J. Chang, C. H. Kuo, Y. K. Su, L. W. Wu, Y. C. Lin, W. C. Lai, J. M. Tsai, G. C. Chi and R. K. Wu, *IEEE Photon. Technol. Lett.*, 2003, **15**, 18–20.
33 V. L. Colvin, M. C. Schlamp and A. P. Alivisatos, *Nature*, 1994, **370**, 354–357.
34 L. Brus, *J. Phys. Chem.*, 1986, **90**, 2555–2560.
35 A. Kortan, R. Hull, R. L. Opila, M. G. Bawendi, M. L. Steigerwald, P. Carroll and L. E. Brus, *J. Am. Chem. Soc.*, 1990, **112**, 1327–1332.
36 T. Takagahara and K. Takeda, *Phys. Rev. B: Condens. Matter Mater. Phys.*, 1992, **46**, 15578–15581.
37 Y. H. Won, O. Cho, T. Kim, D. Y. Chung, T. Kim, H. Chung, H. Jang, J. Lee, D. Kim and E. Jang, *Nature*, 2019, **575**, 634–638.
38 Z. Yang, Q. Wu, G. Lin, X. Zhou, W. Wu, X. Yang, J. Zhang and W. Li, *Mater. Horiz.*, 2019, **6**, 2009–2015.
39 J. Song, O. Wang, H. Shen, Q. Lin, Z. Li, L. Wang, X. Zhang and L. S. Li, *Adv. Funct. Mater.*, 2019, **29**, 1808377.
40 H. Shen, Q. Gao, Y. Zhang, Y. Lin, Q. Lin, Z. Li, L. Chen, Z. Zeng, X. Li, Y. Jia, S. Wang, Z. Du, L. S. Li and Z. Zhang, *Nat. Photon.*, 2019, **13**, 192–197.
41 F. Wang, Q. Hua, Q. Lin, F. Zhang, F. Chen, H. Zhang, X. Zhu, X. Xue, X. Xu, H. Shen, H. Zhang and W. Ji, *Adv. Optical Mater.*, 2022, **10**, 2200319.
42 T. Kim, K. H. Kim, S. Kim, S. M. Choi, H. Jang, H. K. Seo, H. Lee, D. Y. Chung and E. Jang, *Nature*, 2020, **586**, 385–389.
43 C. Liu, W. Li, H. Li, H. Wang, C. Zhang, Y. Yang, X. Gao, Q. Xue, H.-L. Yip, J. Fan, R. E. I. Schropp and Y. Mai, *Adv. Energy Mater.*, 2019, **9**, 1803572.
44 Z. Wang, A. K. Baranwal, M. A. Kamarudin, C. H. Ng, M. Pandey, T. Ma and S. Hayase, *Nano Energy*, 2019, **59**, 258–267.
45 Y. Cao, N. Wang, H. Tian, J. Guo, Y. Wei, H. Chen, Y. Miao, W. Zou, K. Pan, Y. He, H. Cao, Y. Ke, M. Xu, Y. Wang, M. Yang, K. Du, Z. Fu, D. Kong, D. Dai, Y. Jin, G. Li, H. Li, Q. Peng, J. Wang and W. Huang, *Nature*, 2018, **562**, 249–253.
46 K. Lin, J. Xing, L. N. Quan, F. P. G. de Arquer, X. Gong, J. Lu, L. Xie, W. Zhao, D. Zhang, C. Yan, W. Li, X. Liu, Y. Lu, J. Kirman, E. H. Sargent, Q. Xiong and Z. Wei, *Nature*, 2018, **562**, 245–248.
47 N. Wang, L. Cheng, R. Ge, S. Zhang, Y. Miao, W. Zou, C. Yi, Y. Sun, Y. Cao, R. Yang, Y. Wei, Q. Guo, Y. Ke, M. Yu, Y. Jin, Y. Liu, Q. Ding, D. Di, L. Yang, G. Xing, H. Tian, C. Jin, F. Gao, R. H. Friend, J. Wang and W. Huang, *Nat. Photon.*, 2016, **10**, 699–704.
48 Y. Liu, J. Cui, K. Du, H. Tian, Z. He, Q. Zhou, Z. Yang, Y. Deng, D. Chen, X. Zuo, Y. Ren, L. Wang, H. Zhu, B. Zhao, D. Di, J. Wang, R. H. Friend and Y. Jin, *Nat. Photon.*, 2019, **13**, 760–764.
49 H. Zhao, H. Chen, S. Bai, C. Kuang, X. Luo, P. Teng, C. Yin, P. Zeng, L. Hou, Y. Yang, L. Duan, F. Gao and M. Liu, *ACS Energy Lett.*, 2021, **6**, 2395–2403.
50 Y. Hassan, J. H. Park, M. L. Crawford, A. Sadhanala, J. Lee, J. C. Sadighian, E. Mosconi, R. Shivanna, E. Radicchi, M. Jeong, C. Yang, H. Choi, S. H. Park, M. H. Song, F. De Angelis, C. Y. Wong, R. H. Friend, B. R. Lee and H. J. Snaith, *Nature*, 2021, **591**, 72–77.
51 C. Zhang, X. Zhu, F. Gao, L. Yang and W. Liu, *J. Lumin.*, 2022, **244**, 118691.
52 H. Zhang and J. A. Rogers, *Adv. Optical Mater.*, 2019, **7**, 1800936.
53 M. Worku, A. Ben-Akacha, T. Blessed Shonde, H. Liu and B. Ma, *Small*, 2021, **1**, 2000072.
54 S.-J. Woo, J. S. Kim and T.-W. Lee, *Nat. Photon.*, 2021, **15**, 630–634.
55 T.-H. Han, K. Y. Jang, Y. Dong, R. H. Friend, E. H. Sargent and T.-W. Lee, *Nat. Rev. Mater.*, 2022, **7**, 757–777.
56 J. S. Steckel, J. Ho, C. Hamilton, J. Xi, C. Breen, W. Liu, P. Allen and S. Coe-Sullivan, *J. SID*, 2015, **23**, 294–305.
57 S. Nakamura and G. Fasol, *The Blue Laser Diode: GaN Based Light Emitters and Lasers*, Springer-Verlag, 1997.
58 Z. Wang, F. Yuan, X. Li, Y. Li, H. Zhong, L. Fan and S. Yang, *Adv. Mater.*, 2017, **29**, 1702910.
59 A. Žukauskas, R. Vaicekauskas and M. Shur, *Opt. Express*, 2010, **18**, 2287–2295.
60 T. Guner and M. M. Demir, *Phys. Status Solidi A*, 2018, **215**, 1800120.
61 T. M. Brenner, D. A. Egger, L. Kronik, G. Hodes and D. Cahen, *Nat. Rev. Mater.*, 2016, **1**, 15007.
62 Y. Fu, H. Zhu, J. Chen, M. P. Hautzinger, X. Y. Zhu and S. Jin, *Nat. Rev. Mater.*, 2019, **4**, 169–188.
63 V. Naresh, B. H. Kim and N. Lee, *Nano Res.*, 2020, **14**, 1187–1194.
64 Y. Tong, Q. Wang, X. Liu, E. Mei, X. Liang and W. Xiang, *Chem. Eng. J.*, 2022, **429**, 132391.
65 D. Amgar, S. Aharon and L. Etgar, *Adv. Funct. Mater.*, 2016, **26**, 8576–8593.
66 C. Wei, W. Su, J. Li, B. Xu, Q. Shan, Y. Wu, F. Zhang, M. Luo, H. Xiang, Z. Cui and H. Zeng, *Adv. Mater.*, 2022, **34**, e2107798.
67 Y. Wang, X. Liu, Q. He, G. Chen, D. Xu, X. Chen, W. Zhao, J. Bao, X. Xu, J. Liu and X. Wang, *Adv. Funct. Mater.*, 2021, **31**, 2011251.
68 W. Shen, Y. Yu, W. Zhang, Y. Chen, J. Zhang, L. Yang, J. Feng, G. Cheng, L. Liu and S. Chen, *ACS Appl. Mater. Inter.*, 2022, **14**, 5682–5691.
69 Z. Chen, J. Zhao, R. Zeng, X. Liu, B. Zou and W. Xiang, *Chem. Eng. J.*, 2022, **433**, 133195.
70 Y. Lu, Y. Xu, S. Chen, J. Lin, J. Zhu, S. Wang, Y. Zheng, F. Huang and D. Chen, *J. Lumin.*, 2022, **248**, 118952.
71 J. Lin, Y. Lu, X. Li, F. Huang, C. Yang, M. Liu, N. Jiang and D. Chen, *ACS Energy Lett.*, 2021, **6**, 519–528.
72 C. Luo, W. Xia, Z. Ren, D. Shen, Q. Li, Z. Zheng, J. Li, W. Ma and Y. Chen, *Adv. Funct. Mater.*, 2022, **32**, 2113010.
73 Z. Long, S. Yang, J. Pi, D. Zhou, Q. Wang, Y. Yang, H. Wu and J. Qiu, *Ceram. Int.*, 2022, **48**, 35474–35479.
74 Z. Long, H. Ren, J. Sun, J. Ouyang and N. Na, *Chem. Commun.*, 2017, **53**, 9914–9917.

Published on 29 March 2023. Downloaded by Yunnan University on 8/16/2025 4:33:01 AM.

75 X. Li, Y. Wu, S. Zhang, B. Cai, Y. Gu, J. Song and H. Zeng, *Adv. Funct. Mater.*, 2016, **26**, 2435–2445.
76 X. Lin, L. Chen, C. He, Y. Wang, X. Li, W. Dang, K. He, Y. Huangfu, D. Wu, B. Zhao, B. Li, J. Li and X. Duan, *Adv. Funct. Mater.*, 2022, 2210278, DOI: 10.1002/adfm.202210278.
77 D. H. Son, S. M. Hughes, Y. Yin and A. Paul Alivisatos, *Science*, 2004, **306**, 1009–1012.
78 Z. Liu, Y. Zhong, I. Shafei, R. Borman, S. Jeong, J. Chen, Y. Losovyj, X. Gao, N. Li, Y. Du, E. Sarnello, T. Li, D. Su, W. Ma and X. Ye, *Nat. Commun.*, 2019, **10**, 1394.
79 Y. S. Shin, Y. J. Yoon, K. T. Lee, W. Lee, H. S. Kim, J. W. Kim, H. Jang, M. Kim, D. S. Kim, G. Kim and J. Y. Kim, *ACS Appl. Mater. Inter.*, 2020, **12**, 31582–31590.
80 C. Guhrenz, A. Benad, C. Ziegler, D. Haubold, N. Gaponik and A. Eychmüller, *Chem. Mater.*, 2016, **28**, 9033–9040.
81 X. Wang, Y. Yang, X. Li, W. Li, J. Hu and W. H. Zhang, *Opt. Lett.*, 2022, **47**, 593–596.
82 D. Yang, P. Li, Y. Zou, M. Cao, H. Hu, Q. Zhong, J. Hu, B. Sun, S. Duhm, Y. Xu and Q. Zhang, *Chem. Mater.*, 2019, **31**, 1575–1583.
83 Y. Zhang, T. D. Siegler, C. J. Thomas, M. K. Abney, T. Shah, A. De Gorostiza, R. M. Greene and B. A. Korgel, *Chem. Mater.*, 2020, **32**, 5410–5423.
84 C. Otero-Martínez, D. García-Lojo, I. Pastoriza-Santos, J. Pérez-Juste and L. Polavarapu, *Angew. Chem.*, 2021, **60**, 26677–26684.
85 R. Grisorio, E. Fanizza, M. Striccoli, D. Altamura, C. Giannini, I. Allegretta, R. Terzano and G. P. Suranna, *ChemNanoMat*, 2020, **6**, 356–361.
86 D. Chen, S. Zhou, F. Tian, H. Ke, N. Jiang, S. Wang, Y. Peng and Y. Liu, *Adv. Optical Mater.*, 2019, **7**, 1901082.
87 D. Parobek, Y. Dong, T. Qiao and D. H. Son, *Chem. Mater.*, 2018, **30**, 2939–2944.
88 D. Chen, G. Fang, X. Chen, L. Lei, J. Zhong, Q. Mao, S. Zhou and J. Li, *J. Mater. Chem. C*, 2018, **6**, 8990–8998.
89 T. C. Jellicoe, J. M. Richter, H. F. Glass, M. Tabachnyk, R. Brady, S. E. Dutton, A. Rao, R. H. Friend, D. Credgington, N. C. Greenham and M. L. Bohm, *J. Am. Chem. Soc.*, 2016, **138**, 2941–2944.
90 B. Yang, J. Chen, F. Hong, X. Mao, K. Zheng, S. Yang, Y. Li, T. Pullerits, W. Deng and K. Han, *Angew. Chem., Int. Ed.*, 2017, **56**, 12471–12475.
91 F. Zhang, H. Zhong, C. Chen, X. Wu, X. Hu, H. Huang, J. Han, B. Zou and Y. Dong, *ACS Nano*, 2015, **9**, 4533–4542.
92 T.-H. Le, S. Lee, E. Heo, U. Lee, H. Lee, H. Jo, K. S. Yang, M. Chang and H. Yoon, *Chem. Eng. J.*, 2021, **416**, 128045.
93 D. I. Markina, E. Y. Tiguntseva, A. P. Pushkarev, M. A. Samsonov, M. Vengris, B. Munkhbat, T. Shegai, G. B. Hix, A. A. Zakhidov and S. V. Makarov, *J. Lumin.*, 2020, **220**, 116985.
94 M. Chen, H. Hu, Y. Tan, N. Yao, Q. Zhong, B. Sun, M. Cao, Q. Zhang and Y. Yin, *Nano Energy*, 2018, **53**, 559–566.
95 Y. Zhou, K. Fernando, J. Wan, F. Liu, S. Shrestha, J. Tisdale, C. J. Sheehan, A. C. Jones, S. Tretiak, H. Tsai, H. Huang and W. Nie, *Adv. Funct. Mater.*, 2021, **31**, 2101058.
96 A. Varghese, Y. Yin, M. Wang, S. Lodha and N. V. Medhekar, *Adv. Mater. Interfaces*, 2022, **9**, 2102174.
97 X. Hong, Y. Huang, Q. Tian, S. Zhang, C. Liu, L. Wang, K. Zhang, J. Sun, L. Liao and X. Zou, *Adv. Sci.*, 2022, **9**, e2202019.
98 Y. Chen, Y. Jiang, C. Yi, H. Liu, S. Chen, X. Sun, C. Ma, D. Li, C. He, Z. Luo, F. Jiang, W. Zheng, B. Zheng, B. Xu, Z. Xu and A. Pan, *Sci. Chin. Mater.*, 2021, **64**, 1449–1456.
99 X. Yang, R. Wu, B. Zheng, Z. Luo, W. You, H. Liu, L. Li, Y. Zhang, Q. Tan, D. Liang, Y. Chen, J. Qu, X. Yi, X. Wang, J. Zhou, H. Duan, S. Wang, S. Chen and A. Pan, *ACS Nano*, 2022, **16**, 4371–4378.
100 Y. Xu, X. Shi, Y. Zhang, H. Zhang, Q. Zhang, Z. Huang, X. Xu, J. Guo, H. Zhang, L. Sun, Z. Zeng, A. Pan and K. Zhang, *Nat. Commun.*, 2020, **11**, 1330.
101 B. Tang, H. Dong, L. Sun, W. Zheng, Q. Wang, F. Sun, X. Jiang, A. Pan and L. Zhang, *ACS Nano*, 2017, **11**, 10681–10688.
102 X. Wang, H. Chen, H. Zhou, X. Wang, S. Yuan, Z. Yang, X. Zhu, R. Ma and A. Pan, *Nanoscale*, 2019, **11**, 2393–2400.
103 D. N. Dirin, L. Protesescu, D. Trummer, I. V. Kochetygov, S. Yakunin, F. Krumeich, N. P. Stadie and M. V. Kovalenko, *Nano Lett.*, 2016, **16**, 5866–5874.
104 P. Wang, B. Wang, Y. Liu, L. Li, H. Zhao, Y. Chen, J. Li, S. F. Liu and K. Zhao, *Angew. Chem.*, 2020, **59**, 23100–23106.
105 T. Shi, X. Chen, Y. Deng, H. Huang, J. Wang, R. He, Y. Liu, X. He, J. Li, P. K. Chu and X.-F. Yu, *NPG Asia Mater.*, 2022, **14**, 1–12.
106 S. Ye, J. Y. Sun, Y. H. Han, Y. Y. Zhou and Q. Y. Zhang, *ACS Appl. Mater. Inter.*, 2018, **10**, 24656–24664.
107 X. Yu, K. Liu, B. Wang, H. Zhang, Y. Qi and J. Yu, *Adv. Mater.*, 2022, e2208735, DOI: 10.1002/adma.202208735.
108 F. Krieg, S. T. Ochsenbein, S. Yakunin, S. Ten Brinck, P. Aellen, A. Suess, B. Clerc, D. Guggisberg, O. Nazarenko, Y. Shynkarenko, S. Kumar, C. J. Shih, I. Infante and M. V. Kovalenko, *ACS Energy Lett.*, 2018, **3**, 641–646.
109 F. Krieg, Q. K. Ong, M. Burian, G. Raino, D. Naumenko, H. Amenitsch, A. Suess, M. J. Grotevent, F. Krumeich, M. I. Bodnarchuk, I. Shorubalko, F. Stellacci and M. V. Kovalenko, *J. Am. Chem. Soc.*, 2019, **141**, 19839–19849.
110 J. Song, J. Li, L. Xu, J. Li, F. Zhang, B. Han, Q. Shan and H. Zeng, *Adv. Mater.*, 2018, **30**, e1800764.
111 Z. Bao, W. Wang, H.-Y. Tsai, H.-C. Wang, S. Chen and R.-S. Liu, *J. Mater. Chem. C*, 2020, **8**, 1065–1071.
112 J. H. Park, A. Y. Lee, J. C. Yu, Y. S. Nam, Y. Choi, J. Park and M. H. Song, *ACS Appl. Mater. Inter.*, 2019, **11**, 8428–8435.
113 Y. Huang, W. Luan, M. Liu and L. Turyanska, *J. Mater. Chem. C*, 2020, **8**, 2381–2387.
114 L. Yang, B. Fu, X. Li, H. Chen and L. Li, *J. Mater. Chem. C*, 2021, **9**, 1983–1991.
115 Y. Xie, B. Peng, I. Bravic, Y. Yu, Y. Dong, R. Liang, Q. Ou, B. Monserrat and S. Zhang, *Adv. Sci.*, 2020, **7**, 2001698.
116 J. S. Yao, J. Ge, B. N. Han, K. H. Wang, H. B. Yao, H. L. Yu, J. H. Li, B. S. Zhu, J. Z. Song, C. Chen, Q. Zhang, H. B. Zeng, Y. Luo and S. H. Yu, *J. Am. Chem. Soc.*, 2018, **140**, 3626–3634.
117 F. P. Sabino, A. Zunger and G. M. Dalpian, *Mater. Horiz.*, 2021, **9**, 791–803.

 This journal is © The Royal Society of Chemistry 2023

Published on 29 March 2023. Downloaded by Yunnan University on 8/16/2025 4:33:01 AM.

118 J. Jiang, F. Liu, Q. Shen and S. Tao, *J. Mater. Chem. A*, 2021, **9**, 12087–12098.
119 S. Huang, B. Wang, Q. Zhang, Z. Li, A. Shan and L. Li, *Adv. Optical Mater.*, 2018, **6**, 1701106.
120 S. Baek, S. Kim, J. Y. Noh, J. H. Heo, S. H. Im, K.-H. Hong and S.-W. Kim, *Adv. Optical Mater.*, 2018, **6**, 1800295.
121 C. Bi, S. Wang, Q. Li, S. V. Kershaw, J. Tian and A. L. Rogach, *J. Phys. Chem. Lett.*, 2019, **10**, 943–952.
122 C. Luo, W. Li, J. Fu and W. Yang, *Chem. Mater.*, 2019, **31**, 5616–5624.
123 H. Xu, J. Liang, Z. Zhang, Z. Deng, Y. Qiu, M. He, J. Wang, Y. Yang and C. C. Chen, *RSC Adv.*, 2021, **11**, 2437–2445.
124 Y. Hu, X. Zhang, C. Yang, J. Li and L. Wang, *RSC Adv.*, 2019, **9**, 33017–33022.
125 S. Zou, G. Yang, T. Yang, D. Zhao, Z. Gan, W. Chen, H. Zhong, X. Wen, B. Jia and B. Zou, *J. Phys. Chem. Lett.*, 2018, **9**, 4878–4885.
126 H. Shao, X. Bai, H. Cui, G. Pan, P. Jing, S. Qu, J. Zhu, Y. Zhai, B. Dong and H. Song, *Nanoscale*, 2018, **10**, 1023–1029.
127 Y. Liu, G. Pan, R. Wang, H. Shao, H. Wang, W. Xu, H. Cui and H. Song, *Nanoscale*, 2018, **10**, 14067–14072.
128 Y. Shen, J. Yin, B. Cai, Z. Wang, Y. Dong, X. Xu and H. Zeng, *Nanoscale Horiz.*, 2020, **5**, 580–585.
129 I. Lignos, S. Stavrakis, G. Nedelcu, L. Protesescu, A. J. deMello and M. V. Kovalenko, *Nano Lett.*, 2016, **16**, 1869–1877.
130 Q. A. Akkerman, V. D'Innocenzo, S. Accornero, A. Scarpellini, A. Petrozza, M. Prato and L. Manna, *J. Am. Chem. Soc.*, 2015, **137**, 10276–10281.
131 K. Sun, D. Tan, X. Fang, X. Xia, D. Lin, J. Song, Y. Lin, Z. Liu, M. Gu, Y. Yue and J. Qiu, *Science*, 2022, **375**, 307–310.
132 Y. Qian, Y. Shi, G. Shi, G. Shi, X. Zhang, L. Yuan, Q. Zhong, Y. Liu, Y. Wang, X. Ling, F. Li, M. Cao, S. Li, Q. Zhang, Z. Liu and W. Ma, *Sol. RRL*, 2021, **5**, 2100090.
133 Y. Liu, Y. Dong, T. Zhu, D. Ma, A. Proppe, B. Chen, C. Zheng, Y. Hou, S. Lee, B. Sun, E. H. Jung, F. Yuan, Y. K. Wang, L. K. Sagar, S. Hoogland, F. P. Garcia de Arquer, M. J. Choi, K. Singh, S. O. Kelley, O. Voznyy, Z. H. Lu and E. H. Sargent, *J. Am. Chem. Soc.*, 2021, **143**, 15606–15615.
134 L. Yang, J. Huang, Z. Xu, Y. Li, S. Hou, Y. Tan, J. Du, X. Wang, Z. Li and A. Pan, *Adv. Optical Mater.*, 2023, 2202561, DOI: **10.1002/adom.202202561**.
135 W. van der Stam, J. J. Geuchies, T. Altantzis, K. H. van den Bos, J. D. Meeldijk, S. Van Aert, S. Bals, D. Vanmaekelbergh and C. de Mello Donega, *J. Am. Chem. Soc.*, 2017, **139**, 4087–4097.
136 H. Liu, Z. Wu, J. Shao, D. Yao, H. Gao, Y. Liu, W. Yu, H. Zhang and B. Yang, *ACS Nano*, 2017, **11**, 2239–2247.
137 A. Dutta and N. Pradhan, *ACS Energy Lett.*, 2019, **4**, 709–719.
138 X. Zhang, S. Chen, X. Wang and A. Pan, *Small Methods*, 2019, **3**, 1800294.
139 F. Wu, Q. Li, P. Wang, H. Xia, Z. Wang, Y. Wang, M. Luo, L. Chen, F. Chen, J. Miao, X. Chen, W. Lu, C. Shan, A. Pan, X. Wu, W. Ren, D. Jariwala and W. Hu, *Nat. Commun.*, 2019, **10**, 4663.
140 P. Li, Y. Chen, T. Yang, Z. Wang, H. Lin, Y. Xu, L. Li, H. Mu, B. N. Shivananju, Y. Zhang, Q. Zhang, A. Pan, S. Li, D. Tang, B. Jia, H. Zhang and Q. Bao, *ACS Appl. Mater. Inter.*, 2017, **9**, 12759–12765.
141 M. Shoaib, X. Zhang, X. Wang, H. Zhou, T. Xu, X. Wang, X. Hu, H. Liu, X. Fan, W. Zheng, T. Yang, S. Yang, Q. Zhang, X. Zhu, L. Sun and A. Pan, *J. Am. Chem. Soc.*, 2017, **139**, 15592–15595.
142 A. Loiudice, M. Strach, S. Saris, D. Chernyshov and R. Buonsanti, *J. Am. Chem. Soc.*, 2019, **141**, 8254–8263.
143 X. Ren, X. Zhang, H. Xie, J. Cai, C. Wang, E. Chen, S. Xu, Y. Ye, J. Sun, Q. Yan and T. Guo, *Nanomaterials*, 2022, **12**, 2243.
144 H. Xie, E. Chen, Y. Ye, S. Xu and T. Guo, *J. Phys. Chem. Lett.*, 2020, **11**, 1428–1434.
145 H. Xie, E. Chen, Y. Ye, S. Xu and T. Guo, *Appl. Phys. Lett.*, 2020, **117**, 171101.
146 C. Sun, Y. Zhang, C. Ruan, C. Yin, X. Wang, Y. Wang and W. W. Yu, *Adv. Mater.*, 2016, **28**, 10088–10094.
147 Z. Hu, Z. Liu, Y. Bian, S. Li, X. Tang, J. Du, Z. Zang, M. Zhou, W. Hu, Y. Tian and Y. Leng, *Adv. Optical Mater.*, 2018, **6**, 1700997.
148 S. Huang, Z. Li, L. Kong, N. Zhu, A. Shan and L. Li, *J. Am. Chem. Soc.*, 2016, **138**, 5749–5752.
149 W. Yang, F. Gao, Y. Qiu, W. Liu, H. Xu, L. Yang and Y. Liu, *Adv. Optical Mater.*, 2019, **7**, 1900546.
150 C. Rossi, R. Scarfiello, R. Brescia, L. Goldoni, G. Caputo, L. Carbone, D. Colombara, L. De Trizio, L. Manna and D. Baranov, *Chem. Mater.*, 2021, **34**, 405–413.
151 C. K. Trinh, H. Lee, M. G. So and C. L. Lee, *ACS Appl. Mater. Inter.*, 2021, **13**, 29798–29808.
152 X. Tang, W. Chen, Z. Liu, J. Du, Z. Yao, Y. Huang, C. Chen, Z. Yang, T. Shi, W. Hu, Z. Zang, Y. Chen and Y. Leng, *Small*, 2019, **15**, e1900484.
153 W. Chen, J. Hao, W. Hu, Z. Zang, X. Tang, L. Fang, T. Niu and M. Zhou, *Small*, 2017, **13**, 1604085.
154 Z. J. Li, E. Hofman, J. Li, A. H. Davis, C. H. Tung, L. Z. Wu and W. Zheng, *Adv. Funct. Mater.*, 2017, **28**, 1704288.
155 Y. Chen, J. Cai, J. Lin, X. Hu, C. Wang, E. Chen, J. Sun, Q. Yan and T. Guo, *Opt. Lett.*, 2022, **47**, 166–169.
156 M. Lorenzon, M. Jurow, M. J. Hong, Y. H. Lu, E. S. Barnard, M. Salmeron, Y. Liu, E. Penzo, A. M. Schwartzberg and A. Weber-Bargioni, *Adv. Optical Mater.*, 2020, **8**, 2000900.
157 Z. Li, L. Kong, S. Huang and L. Li, *Angew. Chem.*, 2017, **56**, 8134–8138.
158 H. Hu, L. Wu, Y. Tan, Q. Zhong, M. Chen, Y. Qiu, D. Yang, B. Sun, Q. Zhang and Y. Yin, *J. Am. Chem. Soc.*, 2018, **140**, 406–412.
159 C. K. Lin, Q. Zhao, Y. Zhang, S. Cestellos-Blanco, Q. Kong, M. Lai, J. Kang and P. Yang, *ACS Nano*, 2020, **14**, 3500–3508.
160 C. Zou, C. Chang, D. Sun, K. F. Bohringer and L. Y. Lin, *Nano Lett.*, 2020, **20**, 3710–3717.
161 J. Harwell, J. Burch, A. Fikouras, M. C. Gather, A. Di Falco and I. D. W. Samuel, *ACS Nano*, 2019, **13**, 3823–3829.

Published on 29 March 2023. Downloaded by Yunnan University on 8/16/2025 4:33:01 AM.

162 W. Kim, S. K. Kim, S. Jeon, J. Ahn, B. K. Jung, S. Y. Lee, C. Shin, T. Y. Seong, S. Jeong, H. S. Jang, T. N. Ng and S. J. Oh, *Adv. Funct. Mater.*, 2022, **32**, 2111409.
163 J. Liang, K. Wang, Y. Du, C. Zhang, Y. Yan and Y. S. Zhao, *ACS Appl. Mater. Inter.*, 2022, **14**, 1774–1782.
164 K. Wang, Y. Du, J. Liang, J. Zhao, F. F. Xu, X. Liu, C. Zhang, Y. Yan and Y. S. Zhao, *Adv. Mater.*, 2020, **32**, e2001999.
165 X. He, P. Liu, H. Zhang, Q. Liao, J. Yao and H. Fu, *Adv. Mater.*, 2017, **29**, 1604510.
166 S. Li, H. Ding, H. Cai, H. Zhao, Y. Zhao, J. Yang, Y. Jin, N. Pan and X. Wang, *J. Phys. Chem. Lett.*, 2020, **11**, 8275–8282.
167 L. Shi, L. Meng, F. Jiang, Y. Ge, F. Li, X. G. Wu and H. Zhong, *Adv. Funct. Mater.*, 2019, **29**, 1903648.
168 C. Zhang, B. Wang, W. Li, S. Huang, L. Kong, Z. Li and L. Li, *Nat. Commun.*, 2017, **8**, 1138.
169 M. Duan, Z. Feng, Y. Wu, Y. Yin, Z. Hu, W. Peng, D. Li, S. J. Chen, C. Y. Lee and A. Lien, *Adv. Mater. Technol.*, 2019, **4**, 1900779.
170 Z. Gu, Z. Zhou, Z. Huang, K. Wang, Z. Cai, X. Hu, L. Li, M. Li, Y. S. Zhao and Y. Song, *Adv. Mater.*, 2020, **32**, e1908006.
171 Z. Gu, Z. Huang, X. Hu, Y. Wang, L. Li, M. Li and Y. Song, *ACS Appl. Mater. Inter.*, 2020, **12**, 22157–22162.
172 Y. Liu, F. Li, L. Qiu, K. Yang, Q. Li, X. Zheng, H. Hu, T. Guo, C. Wu and T. W. Kim, *ACS Nano*, 2019, **13**, 2042–2049.
173 A. Gao, J. Yan, Z. Wang, P. Liu, D. Wu, X. Tang, F. Fang, S. Ding, X. Li, J. Sun, M. Cao, L. Wang, L. Li, K. Wang and X. W. Sun, *Nanoscale*, 2020, **12**, 2569–2577.
174 C. Paul, *Chem. Mater.*, 2001, **13**, 3299–3305.
175 M. S. Onses, E. Sutanto, P. M. Ferreira, A. G. Alleyne and J. A. Rogers, *Small*, 2015, **11**, 4237–4266.
176 J. U. Park, M. Hardy, S. J. Kang, K. Barton, K. Adair, D. K. Mukhopadhyay, C. Y. Lee, M. S. Strano, A. G. Alleyne, J. G. Georgiadis, P. M. Ferreira and J. A. Rogers, *Nat. Mater.*, 2007, **6**, 782–789.
177 M. Zhu, Y. Duan, N. Liu, H. Li, J. Li, P. Du, Z. Tan, G. Niu, L. Gao, Y. Huang, Z. Yin and J. Tang, *Adv. Funct. Mater.*, 2019, **29**, 1903294.
178 M. Chen, Z. Xu, J. H. Kim, S. K. Seol and J. T. Kim, *ACS Nano*, 2018, **12**, 4172–4177.
179 M. Chen, J. Yang, Z. Wang, Z. Xu, H. Lee, H. Lee, Z. Zhou, S. P. Feng, S. Lee, J. Pyo, S. K. Seol, D. K. Ki and J. T. Kim, *Adv. Mater.*, 2019, **31**, e1904073.
180 Y. Sheng, C. Liu, L. Yu, Y. Yang, F. Hu, C. Sheng, Y. Di, L. Dong and Z. Gan, *Nanoscale*, 2021, **13**, 14450–14459.
181 W. Zhan, L. Meng, C. Shao, X.-G. Wu, K. Shi and H. Zhong, *ACS Photonics*, 2021, **8**, 765–770.
182 J. Chen, Y. Wu, X. Li, F. Cao, Y. Gu, K. Liu, X. Liu, Y. Dong, J. Ji and H. Zeng, *Adv. Mater. Technol.*, 2017, **2**, 1700132.
183 S. Y. Liang, Y. F. Liu, S. Y. Wang, H. Xia and H. B. Sun, *Nanoscale*, 2022, **14**, 1174–1178.
184 C. Zhou, G. Cao, Z. Gan, Q. Ou, W. Chen, Q. Bao, B. Jia and X. Wen, *ACS Appl. Mater. Inter.*, 2019, **11**, 26017–26023.
185 X. Huang, Q. Guo, D. Yang, X. Xiao, X. Liu, Z. Xia, F. Fan, J. Qiu and G. Dong, *Nat. Photon.*, 2019, **14**, 82–88.
186 K. Sun, D. Tan, J. Song, W. Xiang, B. Xu and J. Qiu, *Adv. Optical Mater.*, 2021, **9**, 2100094.
187 M. Li, D. Yang, X. Huang, H. Zhang, Y. Zhao, B. Yin, Q. Pan, J. Kang, N. Zheng, X. Liu, J. Qiu, Z. Yang and G. Dong, *Adv. Mater.*, 2022, **34**, e2201413.
188 Y. H. Song, S. H. Choi, J. S. Yoo, B. K. Kang, E. K. Ji, H. S. Jung and D. H. Yoon, *Chem. Eng. J.*, 2017, **313**, 461–465.
189 H. Wu, S. Wang, F. Cao, J. Zhou, Q. Wu, H. Wang, X. Li, L. Yin and X. Yang, *Chem. Mater.*, 2019, **31**, 1936–1940.
190 X. Shen, C. Sun, X. Bai, X. Zhang, Y. Wang, Y. Wang, H. Song and W. W. Yu, *ACS Appl. Mater. Inter.*, 2018, **10**, 16768–16775.
191 J. He, H. Chen, H. Chen, Y. Wang, S. T. Wu and Y. Dong, *Opt. Express*, 2017, **25**, 12915–12925.
192 H. J. Kim, M. H. Shin, J. Y. Lee, J. H. Kim and Y. J. Kim, *Opt. Express*, 2017, **25**, 10724–10734.
193 F. Li, S. Huang, X. Liu, Z. Bai, Z. Wang, H. Xie, X. Bai and H. Zhong, *Adv. Funct. Mater.*, 2021, **31**, 2008211.
194 Z. Wu, Y. Zhang, B. Du, K. Yang, J. Wu, T. Dai, C. Dong, J. Xia, A. Wu and Z. Zhao, *Nano Energy*, 2022, **100**, 107436.
195 Q. Pan, J. Hu, J. Fu, Y. Lin, C. Zou, D. Di, Y. Wang, Q. Zhang and M. Cao, *ACS Nano*, 2022, **16**, 12253–12261.
196 J. Zhou, F. Huang, H. Lin, Z. Lin, J. Xu and Y. Wang, *J. Mater. Chem. C*, 2016, **4**, 7601–7606.
197 M. N. An, S. Park, R. Brescia, M. Lutfullin, L. Sinatra, O. M. Bakr, L. De Trizio and L. Manna, *ACS Energy Lett.*, 2021, **6**, 900–907.
198 S. Mei, X. Liu, W. Zhang, R. Liu, L. Zheng, R. Guo and P. Tian, *ACS Appl. Mater. Inter.*, 2018, **10**, 5641–5648.
199 T. Wu, C.-W. Sher, Y. Lin, C.-F. Lee, S. Liang, Y. Lu, S.-W. Huang Chen, W. Guo, H.-C. Kuo and Z. Chen, *Appl. Sci.*, 2018, **8**, 1557.
200 X. Zhu, L. Bian, H. Fu, L. Wang, B. Zou, Q. Dai, J. Zhang and H. Zhong, *Light: Sci. Appl.*, 2020, **9**, 73.
201 V. W. Lee, N. Twu and I. Kymissis, *Info. Display*, 2016, **32**, 16–23.
202 H. Chen, G. Tan and S.-T. Wu, *Opt. Express*, 2017, **25**, 33643.
203 J. Bae, Y. Shin, H. Yoo, Y. Choi, J. Lim, D. Jeon, I. Kim, M. Han and S. Lee, *Nat. Commun.*, 2022, **13**, 1862.
204 Y. Li, J. Tao, Q. Wang, Y. Zhao, Y. Sun, P. Li, J. Lv, Y. Qin, W. Wang, Q. Zeng and J. Liang, *Appl. Phys. Lett.*, 2021, **118**, 173501.
205 L. C. Schmidt, A. Pertegas, S. Gonzalez-Carrero, O. Malinkiewicz, S. Agouram, G. Minguez Espallargas, H. J. Bolink, R. E. Galian and J. Perez-Prieto, *J. Am. Chem. Soc.*, 2014, **136**, 850–853.
206 G. Pan, X. Bai, W. Xu, X. Chen, Y. Zhai, J. Zhu, H. Shao, N. Ding, L. Xu, B. Dong, Y. Mao and H. Song, *ACS Appl. Mater. Inter.*, 2020, **12**, 14195–14202.
207 M. Liu, N. Jiang, H. Huang, J. Lin, F. Huang, Y. Zheng and D. Chen, *Chem. Eng. J.*, 2021, **413**, 127547.
208 T. Chiba, Y. Hayashi, H. Ebe, K. Hoshi, J. Sato, S. Sato, Y.-J. Pu, S. Ohisa and J. Kido, *Nat. Photon.*, 2018, **12**, 681–687.
209 J. Kim, K. W. Seo, S. Lee, K. Kim, C. Kim and J. Y. Lee, *Adv. Sci.*, 2022, **9**, e2200073.

 This journal is © The Royal Society of Chemistry 2023

Published on 29 March 2023. Downloaded by Yunnan University on 8/16/2025 4:33:01 AM.

210 D. Chen, P. K. Ko, C. H. A. Li, B. Zou, P. Geng, L. Guo and J. E. Halpert, *ACS Energy Lett.*, 2022, **8**, 410–416.
211 Y. K. Wang, F. Yuan, Y. Dong, J. Y. Li, A. Johnston, B. Chen, M. I. Saidaminov, C. Zhou, X. Zheng, Y. Hou, K. Bertens, H. Ebe, D. Ma, Z. Deng, S. Yuan, R. Chen, L. K. Sagar, J. Liu, J. Fan, P. Li, X. Li, Y. Gao, M. K. Fung, Z. H. Lu, O. M. Bakr, L. S. Liao and E. H. Sargent, *Angew. Chem., Int. Ed.*, 2021, **60**, 16164–16170.
212 S. Sun, M. Lu, Y. Zhong, P. Lu, F. Qin, Y. Gao, X. Bai, Z. Wu and Y. Zhang, *ACS Energy Lett.*, 2022, **7**, 3974–3981.
213 Z. Yao, C. Bi, A. Liu, M. Zhang and J. Tian, *Nano Energy*, 2022, **95**, 106974.
214 D. Zhang, Q. Zhang, B. Ren, Y. Zhu, M. Abdellah, Y. Fu, B. Cao, C. Wang, L. Gu, Y. Ding, K.-H. Tsui, S. Fan, S. Poddar, L. Shu, Y. Zhang, D.-B. Kuang, J.-F. Liao, Y. Lu, K. Zheng, Z. He and Z. Fan, *Nat. Photon.*, 2022, **16**, 284–290.
215 H. Kim, J. H. Park, K. Kim, D. Lee, M. H. Song and J. Park, *Adv. Sci.*, 2022, **9**, e2104660.
216 K. P. Marshall, M. Walker, R. I. Walton and R. A. Hatton, *Nat. Energy*, 2016, **1**, 1–9.
217 L. M. Herz, *ACS Energy Lett.*, 2017, **2**, 1539–1548.
218 J. Lu, X. Guan, Y. Li, K. Lin, W. Feng, Y. Zhao, C. Yan, M. Li, Y. Shen, X. Qin and Z. Wei, *Adv. Mater.*, 2021, **33**, e2104414.
219 J. Luo, X. Wang, S. Li, J. Liu, Y. Guo, G. Niu, L. Yao, Y. Fu, L. Gao, Q. Dong, C. Zhao, M. Leng, F. Ma, W. Liang, L. Wang, S. Jin, J. Han, L. Zhang, J. Etheridge, J. Wang, Y. Yan, E. H. Sargent and J. Tang, *Nature*, 2018, **563**, 541–545.
220 LG. Display, LG Display Unveils High-Performance Gaming OLED Displays at CES 2023, **https://en.prnasia.com/releases/global/lg-display-unveils-high-performance-gaming-oled-displays-at-ces-2023-388948.shtml**, (accessed 2022-12-29, 2023).
221 Samsung, Samsung Semiconductor CES® 2023, **https://semiconductor.samsung.com/cn/event/ces-2023/?cid=cn_pd_display_A_B_C_D_E_F_G&utm_source=A&utm_medium=pd_display&utm_campaign=cn_B_C_D&utm_conte**, (accessed 2023-01-7, 2023).
222 A. Sage, Best of CES 2023: Old Dogs, Not a Ton of New Tricks, **https://www.rollingstone.com/product-recommendations/lifestyle/ces-2023-highlights-lg-sony-samsung-lenovo-1234659610/**, (accessed 2023-01-11, 2023).
223 Macroblock, A Brilliant Driver, Macroblock was on the Road to CES 2023, **https://www.mblock.com.cn/en/newsdetail/330/A%20Brilliant%20Driver,%20Macroblock%20was%20on%20the%20Road%20to%20CES%202023?Open=330**, (accessed 2023-01-06, 2023).
224 D. Sha, CES 2023: Where is the auto tech Wind Blowing? **https://www.sohu.com/a/627132037_166680**, (accessed 2023-01-09, 2023).
225 J. Chen, H. Xiang, J. Wang, R. Wang, Y. Li, Q. Shan, X. Xu, Y. Dong, C. Wei and H. Zeng, *ACS Nano*, 2021, **15**, 17150–17174.
226 H. Wang, X. Gong, D. Zhao, Y.-B. Zhao, S. Wang, J. Zhang, L. Kong, B. Wei, R. Quintero-Bermudez, O. Voznyy, Y. Shang, Z. Ning, Y. Yan, E. H. Sargent and X. Yang, *Joule*, 2020, **4**, 1977–1987.
227 N. Li, A. Feng, X. Guo, J. Wu, S. Xie, Q. Lin, X. Jiang, Y. Liu, Z. Chen and X. Tao, *Adv. Energy Mater.*, 2021, **12**, 2103241.
228 S. Xie, A. Feng, L. Wang, N. Li, X. Cheng, W. Zhang, C. Li, Y. Liu, G. Zhang, X. Du, Y. Fang, Z. Chen and X. Tao, *ACS Materials Lett.*, 2022, **4**, 1332–1340.
229 G. Y. Kim, A. Senocrate, T. Y. Yang, G. Gregori, M. Gratzel and J. Maier, *Nat. Mater.*, 2018, **17**, 445–449.
230 C. C. Boyd, R. Cheacharoen, T. Leijtens and M. D. McGehee, *Chem. Rev.*, 2019, **119**, 3418–3451.
231 F. Giustino and H. J. Snaith, *ACS Energy Lett.*, 2016, **1**, 1233–1240.
232 N. Glück and T. Bein, *Energy Environ. Sci.*, 2020, **13**, 4691–4716.